CAAP Annual Report

Date of Report: 09/30/2025

Prepared for: U.S. DOT Pipeline and Hazardous Materials Safety Administration

Annual Period: From (09/01/2024) to (09/30/2025)

Contract Number: #693JK32350005CAAP

Project Title: Development of a Framework for Assessing Cathodic Protection (CP)

Effectiveness in Pipelines Based on Artificial Intelligence (AI)

Prepared by: TEES (Texas A&M Engineering Experiment Station)

Prof. Homero Castaneda

The University of Dayton, Civil, and Environmental Engineering.

Prof. Hui Wang

Contact Info.: hcastaneda@tamu.edu, phone: 9794589844

Table of Contents

Table of Contents
Section A: Business and Activities
(a) Contract Activities
(b) Financial Summary
(c) Project Schedule Update
Section B: Detailed Technical Results in the Report Period
1. Background and Objectives in the Annual Report Period
1.1. Background 6
1.2. Objectives in the Annual Report Period
2. Theoretical and Experimental Program in the Annual Report Period 7
2.1. Theoretical Deterministic Model Based on Transmission Line Theory
2.2. Experimental Plan 8
2.3. Theoretical, experimental, and field implications of Interfacial Impedance9
3. Results and Discussions
3.1. Task 1: Designing and building the physical prototypes in laboratory conditions and deterministic modeling
3.2. Task 2: Integrating field inspection, theoretical, with experimental data by applying pattern recognition techniques relating the pipeline-coating-soil system with CP 25
3.3. Task 3. Development and validation of the Bayesian machine learning framework with experimental and field conditions
3.4. Task 4 – Development and validation of the methodology for ECDA based on CP levels
4. Future work

Section A: Business and Activities

(a) Contract Activities

Contract Modifications:

No contract modifications have been considered or executed during the second year.

- Educational Activities:
 - Student mentoring:

We organize weekly meetings in the corrosion group for research updates and activities performed. Each student is assigned a PhD student or a Postdoctoral Fellow to follow up on the activities and discuss the results obtained. The students participate in the laboratory activities and conferences (such as AMPP and TAMU internal conferences).

Personalized mentoring with a PhD student or Postdoctoral Fellow to follow up on the student's activities and discuss the results.

o Student internship:

Nothing to report

Educational activities:

We organized an industrial course, Fundamentals, Experiments, and Applications in Corrosion, one of the chapters of which was related to corrosion in pipelines. The course has been offered since 2022.

Career employed:

Nothing to report

• Dissemination of Project Outcomes:

We submitted two abstracts to the AMPP 2026 annual conference, and they were accepted. We have one Research in Progress and one poster for the same conference.

We presented an oral work at Eurocorr 2026 in Norway. We have one PhD thesis that was defended in July 2025.

• Citations of The Publications:

Reece Goldsberry and Homero Castaneda, Characterization and Potential Distribution Mapping of Cathodically Protected Buried Pipelines based on Homogeneous and Heterogeneous Factors, Journal of Pipeline Science and Engineering, https://doi.org/10.1016/j.jpse.2025.100350,

Patent Disclosure

TI Ref. & Title: 6853TEES25- Multi-Scale FEM Electrochemical Model based on

Transmission Line Theory

Inventor(s): Reece Goldsberry, Homero Castaneda-Lopez

(b) Financial Summary

• Federal Cost Activities:

Category	Amount spent during Year 2
	2024-2025
Personnel	\$16,404.02
Faculty	\$33,364.07
PosDoc	NA
Students (RA)	\$649.00
Benefits	\$ 9,271.16
Operating Expenses	\$518.00
Travel	\$493.96
Materials and Supplies	\$300.43
Miscellaneous	\$14,001.53
Subcontracts	\$38,857.60
Indirect costs	\$32,025.33
Total Costs	\$145,885.10

• Cost Share Activities:

- o Cost share contribution:
- Heuristech has contributed \$28,200.00 in technology training and/or company personnel hours for physical laboratory testing and mathematical tools.
- Integrity Solutions has contributed \$86,000 in CP field data collection, technical staff
 resources to collect, collate, evaluate, screening, database development, attending
 workshops and training, analyzing Cathodic Protection (CP) data, contributing to
 computer algorithm development programming, and other program software/model
 components.
- The University of Dayton has contributed \$38,283.38 in cost share, \$25,437.46 in faculty payroll and \$12,845.92 in indirect costs.

(c) Project Schedule Update

• Project Schedule:

Table 1. Timeline and schedule for the project in Gantt chart.

		_			Fisc	al Yea	r					
Task/Subtask	2023		20	24			2025		2025	2026	2026	20
	Q4	Q1	Q2	Q3	Q4	Q1	Q2	Q3	Q4	Q1	Q2	(
Task 1: Designing and building the												
physical prototypes in laboratory												İ
conditions and deterministic modeling												
Task 2: Integrating field inspection,												İ
theoretical with experimental data by												İ
applying pattern recognition techniques												İ
relating the pipeline-coating-soil system												İ
with CP												
Task 3: Validation of the <i>a priori</i>												i
framework with experimental and field												į
conditions for characterization/modeling												İ
and Evaluate/Validate												
Task 4: Development and validation of												
the methodology for ECDA based on CP												
levels												

Deliverable Milestones are indicated in black*

• Corrective Actions:

We have been working on the field testing validation planning during the last quarter, and we will use some pipelines located in the RELLIS campus at Texas A&M. We have two PhD graduates involved in this task.

Task Risk	Priority	Risk Description	Impact Summary	Response Strategy
Select different pipelines for validation of the Methodology. Task 4	Medium to High	-Not finding and using the selected pipelines due to logistics	Identification of pipelines that will allow us to validate the Methodology.	Risk Avoidance RELLIS campus administration will allow the use of the facilities with a proposal.

Section B: Detailed Technical Results in the Report Period

1. Background and Objectives in the 2nd Annual Report Period

Background

Over the past year, we refined the deterministic model based on TLM, which can characterize, quantify, and assess various components of the cathodic protection system. The development of the TLM has become the keystone of the theoretical/experimental/field platform. Different features were added to the TLM-based model to identify low-impedance sites. The TLM model was validated with different field data from different ROW; the validation included the recognition of low impedance sites (rectifiers, anodic bed, coatings holidays). This characterization serves as the baseline for the selected ROW. The TLM model was able to reconcile the laboratory results with the theoretical prediction. A multiscale approach was used in the lab to validate the TLM at the small or micron scale and the laboratory or cm scale. The integration of the laboratory results with the TLM leads the pathway to integration on a macro scale.

A critical step in clustering analysis is determining the optimal number of clusters for a given dataset. Since clustering techniques rely on different data properties, various measures have been proposed to identify the best fit. During this period, we developed advanced methods for analyzing measured cathodic protection (CP) potentials. The CP potential data obtained from a close interval survey (CIS) for the specified region were visualized. Additionally, the metal loss depth, as estimated using an inline inspection (ILI) survey, is aligned with the CP potential data and overlaid for comparison. The analysis reveals a potential correlation between soil heterogeneity and regions of significant metal loss, highlighting the importance of understanding the relationship between soil properties and pipeline integrity. In the last quarter, we were able to integrate clustering and machine learning with the TLM. Finally, the validation of the developed methodology based on ECDA for assessing the cathodic protection will be performed in two ways: the current database for different ROW, and with an existing pipeline. The team found a steel pipeline located at the RELLIS campus of Texas A&M University.

Objectives in the Annual Report Period

OBJECTIVES

The herein proposal includes the following objectives:

- Develop a unique experimental-mathematical modeling platform with field data-driven that will serve as an external corrosion assessment tool for the identification and quantification of CP effectiveness.
- Reduce the likelihood of incidents related to failures caused by corrosion, thus boosting the overall integrity of pipeline systems,
- Enhance the identification, quantification, and assessment of anomalies, elements of the pipeline, and CP elements via deterministic, data-driven, and artificial intelligence.
- Perform standard measurement pipeline monitoring techniques for validation of a developed CP model

2. Theoretical and Experimental Program in the Annual Report Period

2.1 Theoretical Deterministic Model Based on Transmission Line Theory

In continued efforts to create a deterministic model for modeling the potential distribution in cathodically protected pipelines, validation was performed both on the lab and field scale. Validation on the lab scale was continued by comparing the output of the 2D TLM using mechanistic definitions for the interface impedance with experimental data. To begin validating the model in the larger field scale, the initial model was extended to a quasi-1D case where the x-direction of the model (length of the pipeline) is on the order of kilometers while the y-direction (circumference of the pipeline) is on the order of meters. After validation, the model was then extended to be able to accurately simulate the potential distribution under more complex and dynamic conditions. Key enhancements include the incorporation of temporal variations in soil regime based on seasonal shifts, the multi-scale modeling of electrical bonding between pipelines, and localized interfacial impedance adjustments based on defects present in the coating. These local simulations enable multiscale features to be integrated within a coarser global framework for enhanced physical accuracy and real-world applicability.

Theoretical Deterministic Model coupled with the Machine Learning model Framework

The transmission-line model (TLM) was developed by the Texas A&M team to numerically compute the potential distribution along the soil—pipeline interface, taking into account the spatial heterogeneity. However, variability in soil resistivity, coating impedance, and other environmental factors introduces uncertainty that purely physics-based models cannot fully capture. To address this, we developed and implemented a physics-informed and uncertainty-aware Bayesian digital twin for pipeline external corrosion assessment, which couples a physics-based transmission-line model (TLM) with a Bayesian probabilistic updating framework. By integrating high-fidelity numerical simulation of the pipeline-soil interface with probabilistic inference, the digital twin yields spatially resolved predictions of coating interfacial impedance and assesses cathodic protection (CP) effectiveness, along with quantified uncertainty. The proposed approach, as shown in **Figure 1**, enhances traditional external corrosion direct assessment (ECDA) by accounting for heterogeneous soil and coating properties, enabling more reliable severity estimates and informed maintenance planning.

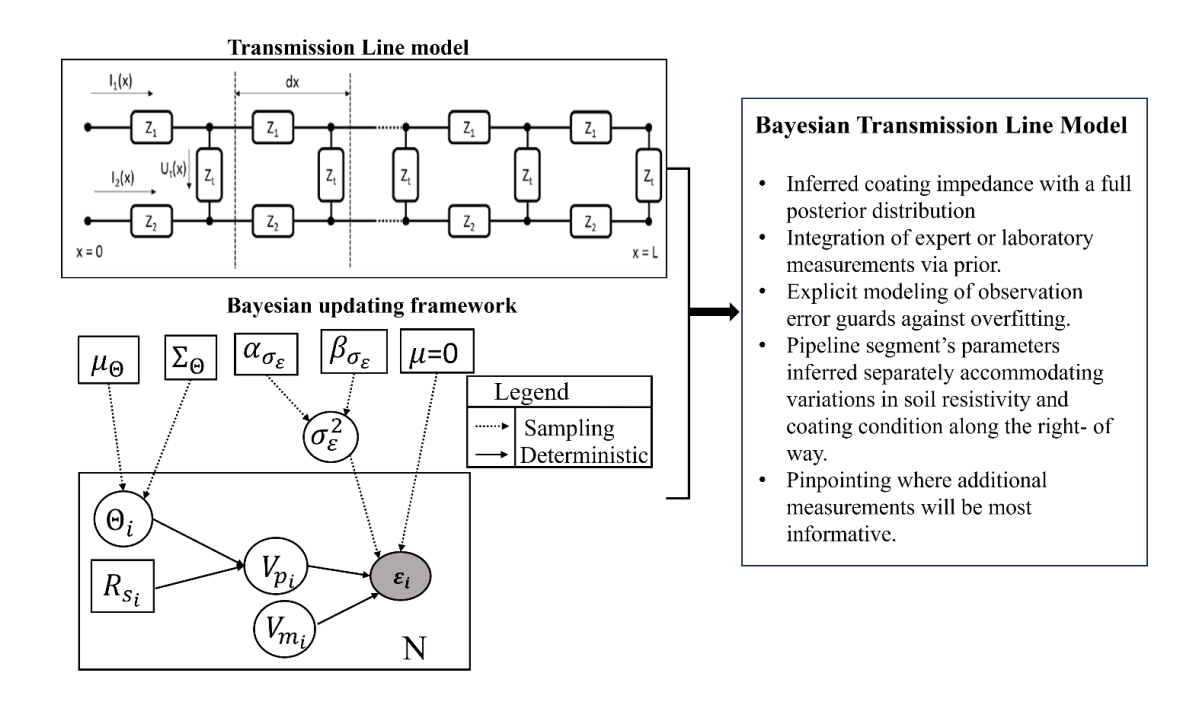


Figure 1: Proposed framework for Bayesian Transmission Line Model

2. 2 Experimental Plan

Continued laboratory testing involves validating a deterministic model for cathodic protection (CP) systems through two distinct laboratory-scale experiments, aiming to extend the model's accuracy across multiple length scales and extend to two dimensions. The first validation case (**Figure 2**) focuses on measuring the two-dimensional potential distribution in a scaled-down system that incorporates real-world complexities like electrical bonding between pipelines, complex geometries, and external AC/DC interferences. This setup uses carbon steel pipes with Fusion-Bonded Epoxy (FBE) coating buried in soil. The second validation case (**Figure 3**) investigates the impact of CP polarization on the degradation of applied coatings. Coated panels will be exposed to environmental factors, either under CP or natural aging, and their resulting electrochemical properties will be measured using Electrochemical Impedance Spectroscopy (EIS). The data from both cases will be used to refine the model, especially by defining the interfacial impedance for aged coatings, ultimately building confidence in the model's ability to simulate real-world CP systems.

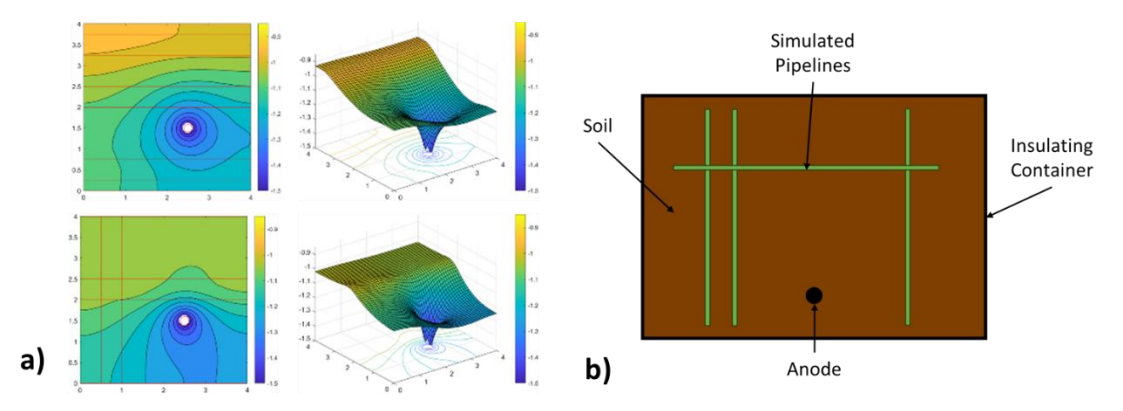


Figure 2: a) Numerical simulation of a two-dimensional potential distribution for an arbitrary pipeline network with singular anode placement, and b) Small-scale physical model of pipeline network

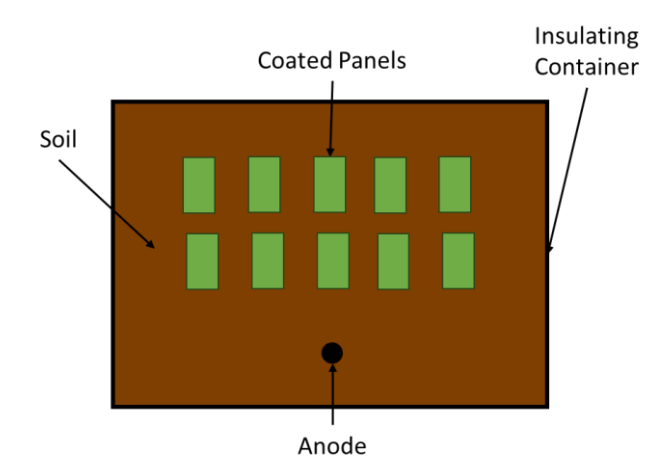


Figure 3: Physical setup for testing the effectiveness of CP on aged coating panels

Theoretical Deterministic Model

2.3 Theoretical, experimental, and field implications of Interfacial Impedance

Both mechanistic and traditional electrical equivalent circuit (EEC) definitions can be used when defining the interfacial impedance in the TLM Potential Distribution model. A summary of the EEC definitions and mechanistic definitions is shown in **Tables 1 and 2**, respectively.

Table 1: Traditional EEC Definitions

Electrical Element	Impedance Form	Use
R	$Z_R = R$	Charge Transfer Processes
C	$Z_C = \frac{1}{i\omega C}$	Capacitive Processes

СРЕ	$Z_{CPE} = \frac{1}{(i\omega)^n Q}$	Capacitive Processes with assumed heterogeneities at the interface
Warburg Impedance ^{1,2}	$Z_W = \sigma_W (i\omega)^{-1/2}$	Diffusion Processes

Table 2: Mechanistic Impedance Definitions

Mechanism	Impedance Form
Coating Capacitance: Ideal	$C_C = \frac{\epsilon_0 \epsilon_r A}{t}$
Coating Capacitance: Double Layer ^{3,4,5,6,7}	$Z(\omega) = \delta \frac{\rho_c}{1 + i\omega\tau} - \frac{\lambda}{i\omega\epsilon_0\epsilon_r} \ln\left(\frac{1 + i\omega\tau\exp(-\frac{t - \delta}{\lambda})}{1 + i\omega\tau}\right)$ $\tau = \epsilon_0\epsilon_r\rho_c$
Coating Resistance	$R_C = \frac{\rho_C t}{A}$
Double Layer Capacitance ⁸	$C_{dl} = \left(\frac{1}{C_H} + \frac{1}{C_{diff}}\right)^{-1}$ $C_H = \frac{\epsilon}{4\pi d}$ $Q_d = -\left[2\epsilon RT \sum_i c_i^0 \left(\exp\left(\frac{z_i F \psi_0}{RT}\right) - 1\right)\right]^{\frac{1}{2}}$ $C_{diff} = -\frac{dQ_d}{d\psi_0}$
Charge Transfer Resistance	$i = i_0 \exp(b(E - E_0))$ $\tilde{\iota} = \bar{\iota}b\tilde{E}$ $\bar{\iota} = i_0 \exp(b(\bar{E} - E_0))$ $R_{ct} = \left(\frac{\tilde{E}}{\tilde{\iota}}\right) = \frac{1}{i \cdot b}$

3. Results and Discussions

Task 1: Designing and building the physical prototypes in laboratory conditions and deterministic modeling

Validation of TLM Potential Distribution Model

Verification with Analytical Solution

Firstly, the model's output was compared with commonly used analytical solutions for describing the potential decay seen in cathodically protected pipelines. **Equations 1 – 4** are used to calculate the potential decay for an infinite or finite pipeline with a length of 2l respectively⁹⁻¹¹. The ending boundary condition infinite pipeline was such that as the pipeline went to infinity eventually the assumed potential would be equal to zero and for the finite pipeline at the end of the pipeline (x = 1) the potential is equal to E_m or more simply it could be assumed that the current will be zero (dE/dx = 0).

$$E_{inf} = E_A e^{-\alpha x} \tag{1}$$

$$E_{fin} = E_m \cosh(\alpha(l-x))$$
 (2)

$$\alpha = \sqrt{R_s/R_c} \tag{3}$$

$$E_A = E_m \cosh(\alpha l) \tag{4}$$

Where R_s is the soil resistance per length, R_c is the coating resistance per length, α is the attenuation coefficient, E_A is the applied potential, and E_m is the assumed minimum potential to still provide protection. For both pipelines, the boundary condition at the at the drainage point (x = 0) was assumed to be equal to E_A . Figure 4 compares of the model's output with analytical expression for potential distribution in pipelines, it was assumed that the coating and soil properties were held constant for the entire length of the pipeline for both pipeline cases.

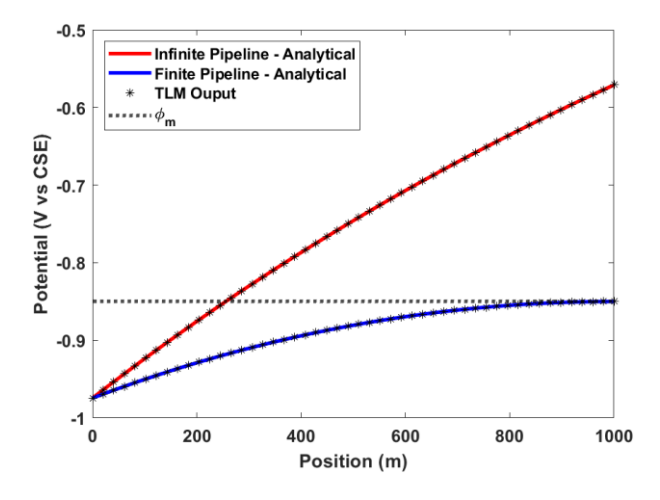


Figure 4: Comparison of the TLM model output with analytical expression for potential distribution in pipelines

Figure 4 illustrates that the output of the model aligns completely with the potential decay described by the two analytical solutions. This result demonstrates the model's capability to accurately predict the potential distribution in the simplest scenarios, thereby validating its effectiveness and reliability in handling fundamental cases.

Validation with Field CIPS

To validate the proposed TLM, the model's output was compared with the on-potentials measured using CIPS. The measured soil resistivity along the length of the pipeline and applied potential values at rectifier sites were taken from the field data, and the coating resistivity values along the pipeline were assumed to provide the best fit between the model and field data. Comparable to the numerical analysis performed it was assumed that the coating properties were distributed along the length of the pipeline. The RSD value was varied to find the best fit between the model output and field CIPS data to incorporate any possible heterogeneities that could occur in the system. The model's output was only used to follow the general trend of the field CIPS measurements since the model does not incorporate any possible measurement or instrument error. Figure 5 and 6 show the measured soil resistivity, assumed interface coating impedance magnitude, and the comparison between the model output and field data for two different pipelines.

The first pipeline (**Figure 5**) used was 56 km section of pipeline with two potential application sites at 431.76 km and 471.61 km with values of -1.76 V vs CSE and -2.24 V vs CSE. The soil resistivity for the pipeline could be split into two regions, with the first region from 426 km to around 452 km and the second region from around 452 km to 483 km. The first region had a large variation from point to point in the measured resistivity ranging from $10^3 - 10^5 \Omega$ -cm while in the second region the resistivity was much more stable with values around $10^3 - 10^4 \Omega$ -cm. For the second pipeline (**Figure 6**) a 112 km section with multiple potential application sites was used for validation. The location and potential values were included in **Table 3**. The soil resistivity for the pipeline was relatively constant over the length of the pipeline most values were around $10^3 - 10^4 \Omega$ cm but past 60km the overall soil resistivity values steadily increased.

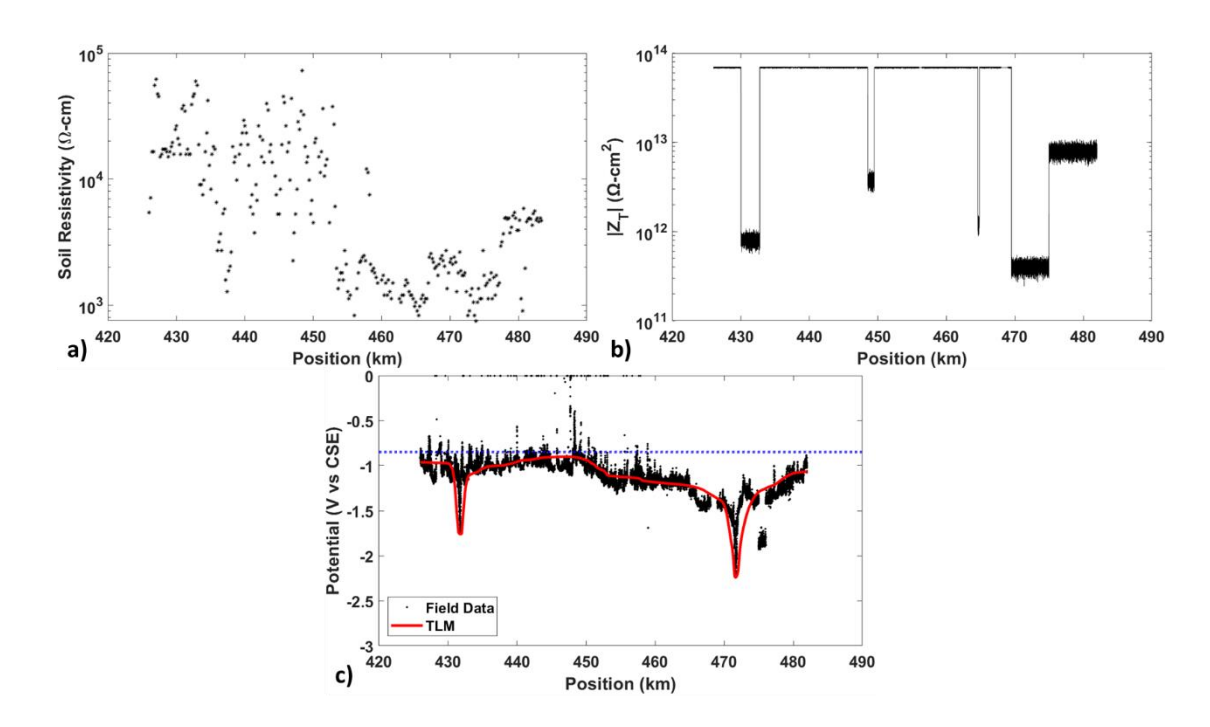


Figure 5: a) Measured soil resistivity versus location, b) assumed interface impedance magnitude versus location, and c) comparison between the model's output with the measured on-potentials. The Blue dashed line is the minimum assumed protection potential (-0.850 V vs CSE)

Table 3: Pipeline 2's rectifier location and applied potential

Rectifier Location current drainage	Applied Potential
(km)	(V vs CSE)
1.632	-1.4841
4.74	-1.5527
24.25	-1.842
26.92	-2.1001
42.11	-2.0105
47.57	-1.6497
52.39	-1.5683
68.97	-1.7491
90.18	-2.0524
100.41	-2.4861
111.58	-3.6703

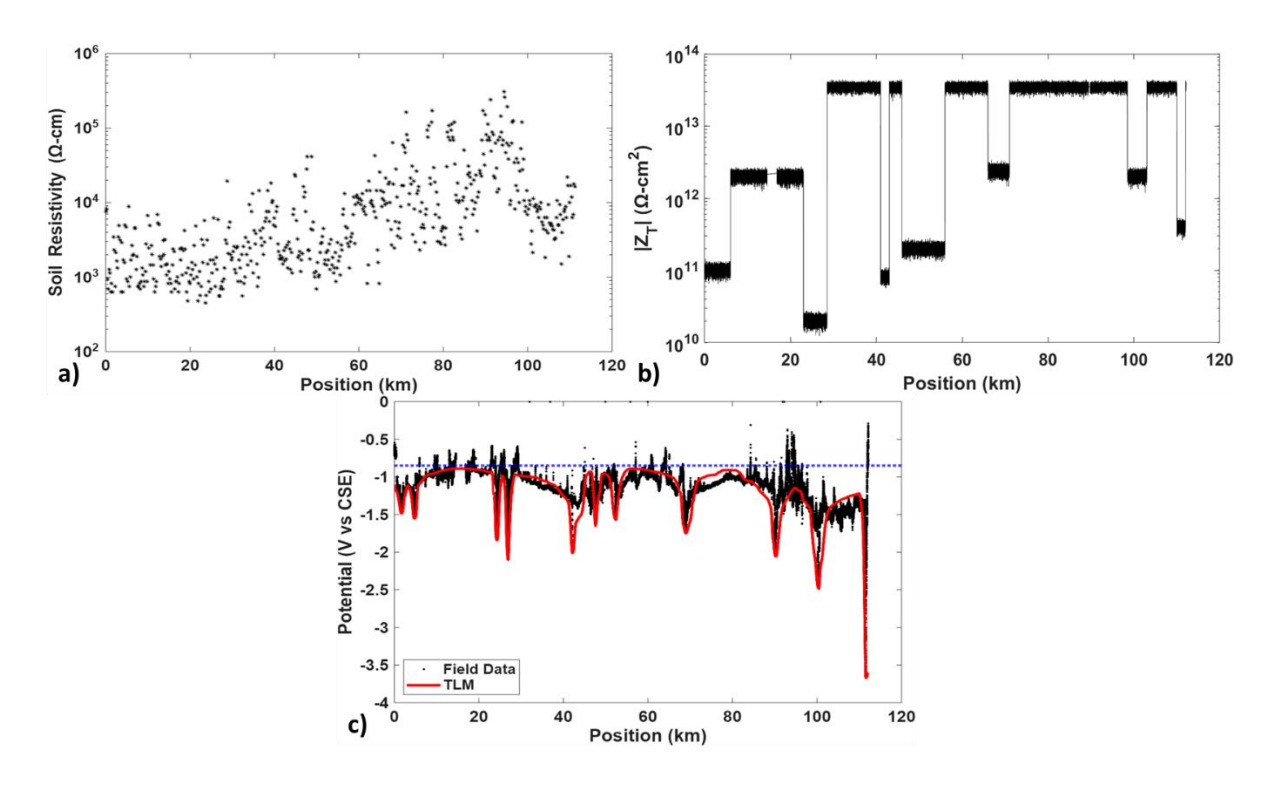


Figure 6: a) Measured soil resistivity versus location, b) assumed interface impedance magnitude versus location, and c) comparison between the model's output and the measured on-potentials. Blue dashed line is the minimum assumed protection potential (-0.850 V vs CSE)

Figure 5b and **Figure 6b** display the impedance distribution along the length of the pipelines. From the plots, it can be seen that in the area surrounding rectifiers, there seemed to be a consistently lower overall impedance in these regions compared to the impedance of the rest of the pipeline. A plausible reason for the impedance decrease is likely due to the accelerated aging that can occur in coatings under higher levels of cathodic protection ^{12,13}. Since the applied potential at the rectifier is known along with the resistivity values in the area, the only way to account for the sharp rise in the measured potentials to more positive values would be from a decreased impedance in the local area. To account for the lower impedance in regions relatively farther away from the rectifiers, multiple factors can cause a decrease in interfacial impedance, including a decrease in coating resistivity due to water uptake, chemical degradation of the coating, and the presence of defects in the coating. Water uptake and chemical degradation of the coating are slow processes that affect the coating impedance over time. This form of degradation would typically only cause a relatively small but measurable change in the overall impedance of the system. In the most extreme cases, where there is bare metal exposed, the overall impedance changes would be very large over multiple orders of magnitude difference between locations due to the exposure of the bare substrate. The ability of the model to pick and differentiate between the possible accelerated degradation by the rectifiers and the damage that can occur naturally along the pipe depends on the CIPS measurement resolution. With increasing distance between measurement points, the total surface area that is being surveyed drastically increases.

Simulation of Electrical Bonding in Parallel Pipelines

Figure 7 shows a simplified example of electrical bonding between parallel pipelines that was used to develop the true geometries used in the simulation. However, these drawings do not reflect the actual spatial dimensions used in the model.

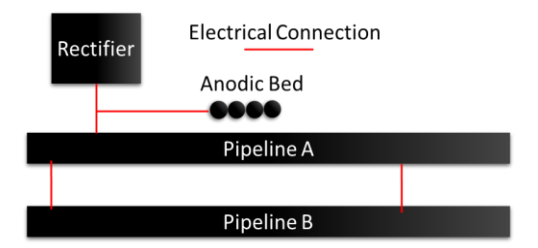


Figure 7: Simple example displaying the electrical bonding in parallel pipelines exposed to the same CP system

For both simulation cases, it was assumed that the pipeline had a diameter of 0.5 m (~20") and was coated with a fusion-bonded epoxy (FBE). To simulate electrical bonding, it was assumed that the electrical connection was made with a #4 AWG wire ($\emptyset_{wire} = 0.005 \text{ m}$) and that the bonding wire was coated with a perfectly insulating coating. For the parallel pipeline condition, it was assumed that the drainage point (rectifier location) was positioned at the left boundary of pipeline 1. It was assumed that the modeled domain was a small portion of two infinitely long pipelines. Accordingly, with this assumption, the boundary conditions for the right boundary of pipeline 1 and both boundaries of pipeline 2 were defined such that the current approaches zero at infinity in each direction. The modeled domain was adjusted for multiple simulations by altering the assumed pipeline length and the configuration of bonding sites.

Figures 8 and 9 present two case studies used to simulate the multi-scale challenge of electrical bonding of pipelines under the shared CP system. **Figure 8** clearly illustrates that the placement of the initial bonding site is important in the level of cathodic protection applied to the second pipeline (without a CP system) as well as the deviation of the system from the isolated pipeline case. As the number of bonding sites increases, the calculated potential difference between the two pipelines consistently decreases, indicating enhanced electrical continuity and reduced CP disparity. However, the observed maximum differential, ranging between 1 to 2 mV, is minimal and likely indistinguishable in practical field measurements, where such subtle variations could be obscured by system noise and measurement error. Despite this, the trend remains significant in modeling contexts, as it underscores the sensitivity of pipeline interaction to bonding configuration and density. To further tests the model's ability to include bonding effects the length of the pipelines was increased to more realistic distances on the order of km.

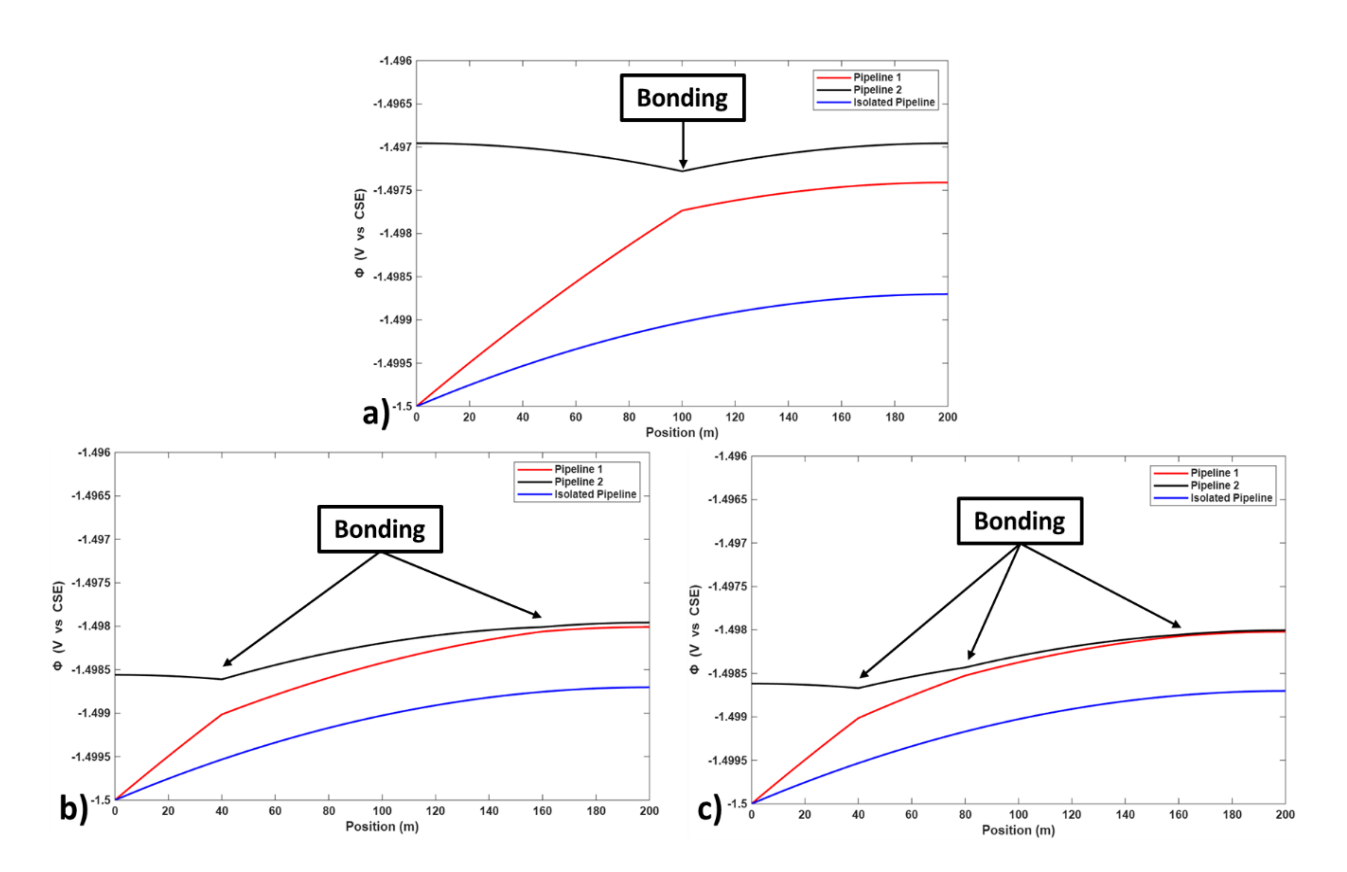


Figure 8: Comparison of the number and location of bonding sites on the potential distribution for cathodically protected pipelines, a) single bonding site (100m), b) two bonding sites (40m and 160m), and c) three bonding sites (40m, 80m, and 160 m)

Figure 9 shows the simulation of longer pipeline segments to allow for a better understanding of how these bonds can affect potential distributions on a real-world scale. For this simulation, the soil resistivity was assumed to be homogenous across the domain and set to a value of 1e4 Ω cm. There were two model configurations consisting of two 10 km and 100 km pipelines separated by 4 meters, with two different bonding locations. For the 10 km pipelines, an initial connection was located at 1km, and for the 100 km pipelines, the location was set to 50 km.

Figure 9 further reinforces that the bonding site functions as an equipotential node between the two pipelines, effectively equalizing the electrical potential at this connection point. In the second pipeline, these bonding sites act analogously to drainage points in a CP system, like those observed in pipeline 1 (x = 0). The potential distribution along the second pipeline exhibits the expected exponential decay, characteristic of CP-influenced systems. Notably, downstream of the bonding site, pipeline 1 mirrors this same decay profile, indicating a shared electrical behavior post-connection. However, upstream of the bonding location, pipeline 1 displays a steeper potential gradient than anticipated. Providing another way of showing the need for proper electrical continuity when applying CP for more complex systems. Overall, the model successfully captures the nuanced potential distribution across electrically bonded pipeline systems, validating its applicability for simulating real-world CP interactions.

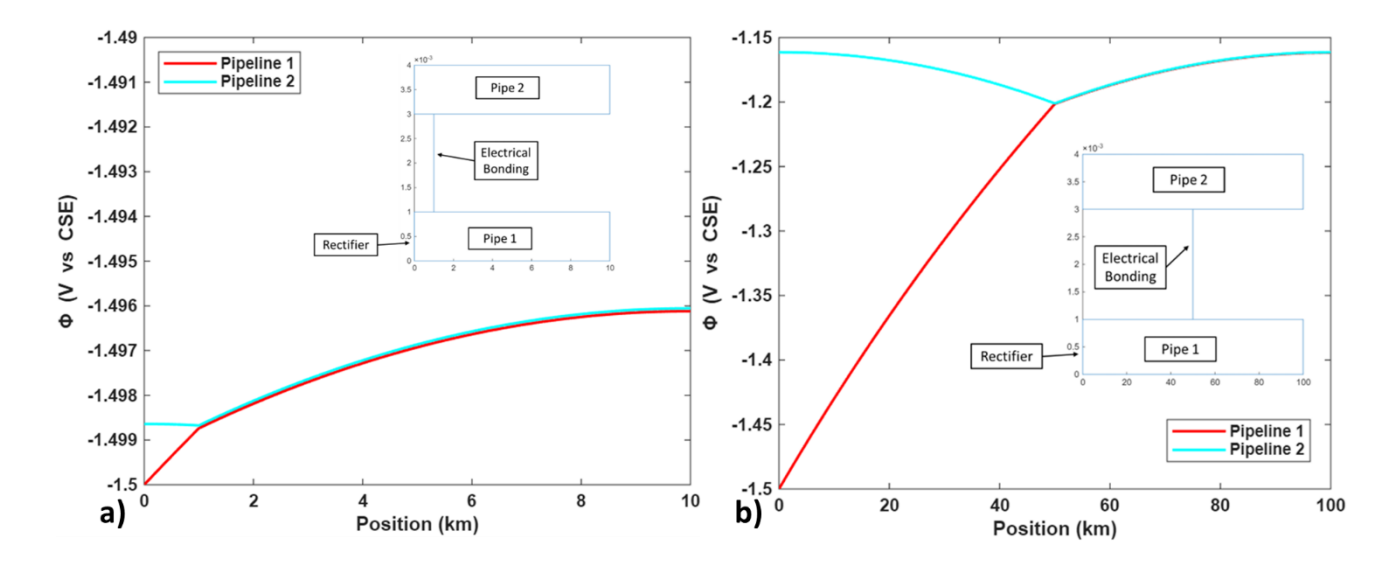


Figure 9: Expansion of the model to include larger lengths of pipelines a) 10km pipeline with single bonding location at 1km, and b) 100km pipeline with single bonding location at 50 km.

Spatial and Time Variation of Soil Resistivity

Soil is an inherently heterogeneous electrical medium that consists of three distinct phases, and the resistivity is primarily dependent on the liquid phase present, since the resistivity is based on the ion-ion interactions and electrolytic theory^{14,15}. Common soil resistivity values typically fall into the range of 10^2 - 10^7 Ω -cm depending on various factors (location, time of year, and composition)¹⁶. It is common for there to be some seasonal fluctuation in the soil resistivity due to the changes in moisture content and temperature of the soil, depending on the time of the year. Relationships can be made to understand the changes in the apparent soil resistivity depending on the moisture content, temperature, and composition 17-19. The spatial variation of soil resistivity was modeled using a lognormal distribution, reflecting the fact that resistivity values are strictly positive and typically exhibit asymmetry around the mean. To simulate different levels of variability within the system, the relative standard deviation (RSD) was used in the description of the distribution parameters. **Equation 5** represents the soil resistivity model used in this model that considers the spatial and temporal variations. The spatial variation in **Equation 6 – 10** is a lognormal distribution with the individual terms, and **Equation 6** presents a simplified empirical model for simulating annual fluctuations in the soil resistivity driven by cyclical environmental changes.

$$P_{soil} = Spatial\ Variation + Temporal\ Variation$$
 (5)

Spatial Variation
$$\sim lognormal(\mu, \sigma^2)$$
 (6)

$$\mu = \ln\left(\frac{\rho_{soil}}{\sqrt{\rho_{soil}^2 + \sigma_{soil}^2}}\right)$$
(7)
$$\sigma^2 = \ln\left(1 + \frac{\rho_{soil}^2}{\sigma_{soil}^2}\right)$$
(8)

$$\sigma^2 = \ln\left(1 + \frac{\rho_{soil}^2}{\sigma_{soil}^2}\right) \tag{8}$$

$$\sigma_{soil} = \rho_{soil} * RSD_{soil} \tag{9}$$

Temporal Variation =
$$A\cos(\omega(t-t_0))$$
 (10)

Where P_{soil} is the total combination of the soil resistivity in Ω -cm. For the spatial variation μ and σ are the lognormal distribution parameters, ρ_{soil} is the mean values of the soil resistivity for the region, σ_{soil} is the standard deviation of the resistivity and is assumed to be related to ρ_{soil} by RSD_{soil} which is the assumed relative standard deviation of the soil. For the cyclical variation A is the magnitude of the cyclical variation, ω is the angular frequency, t is the time in months, and t_0 is the phase shift value.

For understanding how the spatial and time variation of soil resistivity plays a role in the overall potential distribution for CP systems. It was assumed that the pipeline modeled was a 125 km pipeline with a FBE coating with a mean coating resistivity of 1e15 Ω cm and a 1% RSD of coating resistivity, relative permittivity of 3, and thickness of 400 μ m. The average interfacial impedance of this coating was calculated to be 4e13 Ω cm². These assumed pipelines were used in both potential distribution profiles shown in **Figure 10c** and **Figure 11**.

Figure 10a and 10b illustrate the spatial and time variation of the soil resistivity, respectively. For the spatial profile, a mean resistivity value of 5e3 Ω cm was assumed, with an RSD of 20% to account of natural heterogeneities that occur in the soil phase. Temporal variation was modeled using the empirical relationship shown in **Equation 6**, incorporating a sinusoidal fluctuation amplitude of the variation of 1e3 Ω cm. The phase shift was such that the resistivity peaked in the middle of the year, corresponding to drier and warmer months. Although the empirical model is simplistic, it captures the dominant seasonal trend and is sufficient for this analysis. It was assumed that the and that Since temporal variation was cyclical, it was chosen only to simulate two conditions. The boundary cases were selected to capture the extremes of soil behavior and assess their impact on the CP performance under varying environmental conditions.

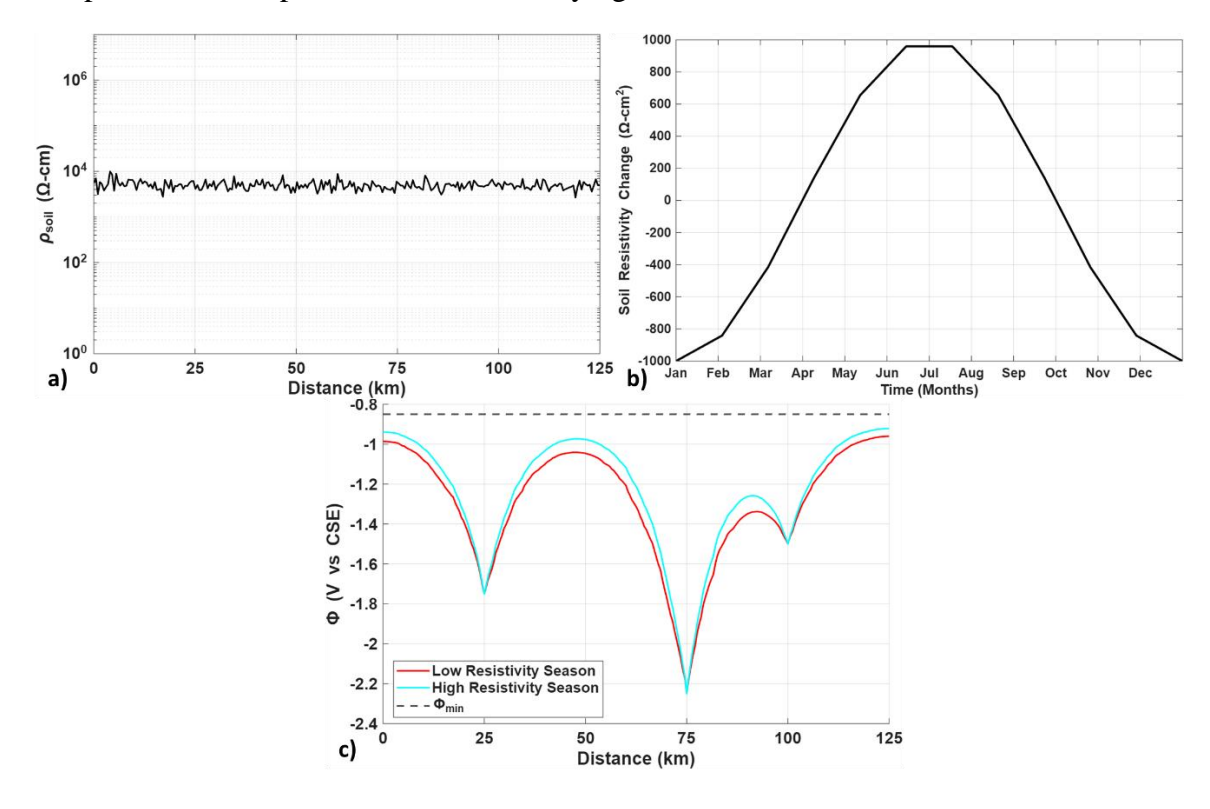


Figure 10: a) Spatial and b) Temporal distribution of the soil resistivity, and c) Calculated potential distribution at different assumed seasons.

Figure 10c provides a visualization of the role of cyclical soil effects on the potential distribution in cathodically protected pipelines. The shift in the potential profile based on the season can have an impact on the effectiveness of the CP system. If sacrificial anodes are used, then large seasonal shifts in the soil resistivity can drastically reduce the anodes' ability to protect the substrate in times of higher soil resistivity. The use of impressed current systems can overcome this shift, but care must be taken to ensure not to over-polarize the system and increase the risk of cathodic disbondment and hydrogen embrittlement of the pipeline. The variation observed in the potential profiles from **Figure 10c** prompted further investigation into the sensitivity of the potential distributions with different mean resistivity values and cyclical amplitudes. **Figure 11** presents the resulting potential profiles for two systems, each characterized by distinct mean resistivity levels and swing amplitudes.

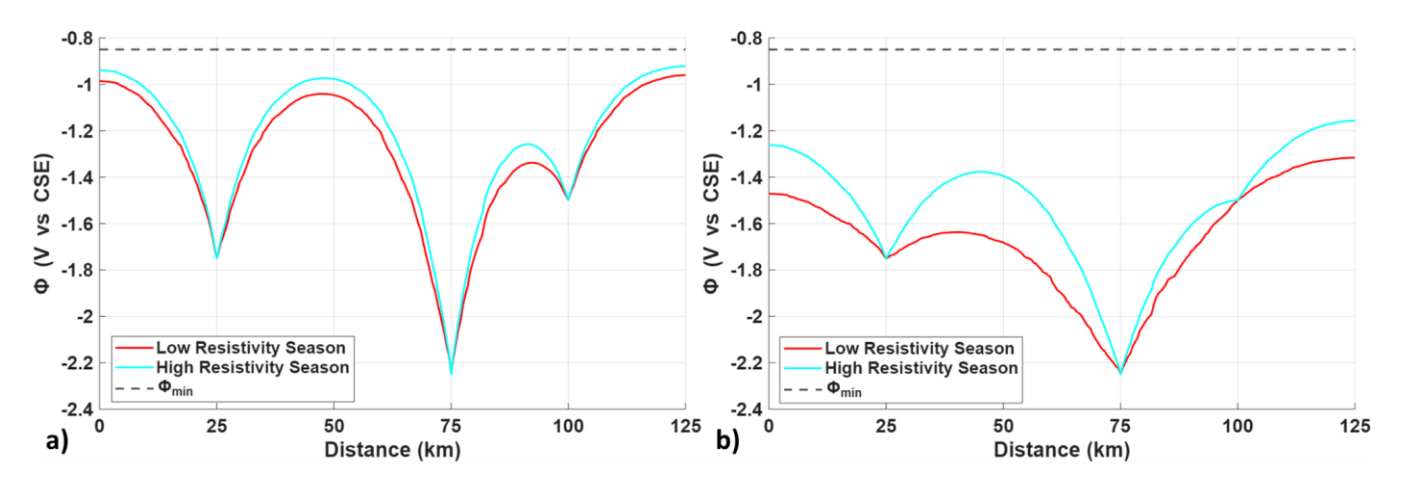


Figure 11: Comparison of the potential distribution under the high and low resistivity season for a) mean soil resistivity 5e3 with 1e3 cyclical amplitude and b) mean soil resistivity 1e3 and 5e2 cyclical swing

As shown in **Figure 11**, the impact of seasonal fluctuations is highly sensitive to the underlying mean soil resistivity of the system. It is clear that the higher resistivity region is less sensitive to the assumed seasonal fluctuations as compared to the lower resistivity region. This can also be seen in the calculated residuals between the high and low resistivity seasons for the two regions shown in **Table 4**.

Table 4: Quantitative Comparison of Potential Residuals Between the Season

Region	Max (V vs CSE)	Min (V vs CSE)	Average (V vs CSE)
High Resistivity Region	0.106	1.8e-6	0.058
Low Resistivity Region	0.292	2.3e-6	0.150

For the high resistivity region, the maximum difference in the potential profiles was around 100 mV vs CSE, while for the lower resistivity region, the maximum difference nearly tripled to around 290 mV vs CSE. This increased sensitivity to seasonal fluctuations in low-resistivity regions must be carefully considered when designing and installing a CP system. Larger seasonal swings in the potential profile can result in misestimating the required level of protection, potentially leading to under-protection, and allowing corrosion to propagate unchecked.

Effect of Holiday Activity and Feature Size on Defect Detection

Detecting defects in pipeline coatings requires either a measurable change in pipe-to-soil potential (as in CIPS), a detectable gradient in the system's potential distribution (DCVG/ACVG), current attenuation analysis, or in-line inspection techniques. All of these methods depend on high-resolution surveys capable of identifying small-scale anomalies. When modeling relatively long pipeline segments (>50 km), mesh validity becomes a challenge. Simulating localized defects, often on the order of centimeters, within a coarse mesh can lead to numerical instability and incoherent results. To address this, a two-tiered modeling approach is employed: a coarse global model is first used to compute the general potential distribution across the pipeline. Then, targeted high-resolution sub-models (~100 m in length) are applied to specific regions to resolve local potential, transverse current, and interfacial impedance distributions. The averaged interfacial impedance values from these refined sub-models are then reintegrated into the coarse model, enabling a simplified yet representative simulation of regions with possible defects.

The system used for the high-resolution sub-model was a 100m length of pipeline with defects of various sizes and activities located in the center of the simulated region. To assign the boundary conditions of the model, the potential at the edges of the sub-model was set to the same values obtained in the initial macro-scale simulation. The soil resistivity was the same over the sub-model domain as in the coarse model. A summary of the holiday activity and sizes is shown in **Table 5**.

Table 5: Over view of sub-model parameters

Model Parameter	Values
Holiday Radius	1, 10, 50 cm
Holiday R _{ct}	1e8, 1e5, 1e2 Ωcm ²

Three holiday sizes were selected to span a range from small to large with areas varying from 10^0 cm² to 10^3 cm². Correspondingly, three activity levels were defined to represent different surface conditions that may occur at the pipeline surface. If we assume that the anodic and cathodic reactions occurring at the interface were shown by **Equations 11 and 12** respectively²⁰:

$$Fe \rightarrow Fe^{2+} + 2e^{-}$$
 (11)
 $2H^{+} + 2e^{-} \rightarrow H_{2}$ (12)

Focusing on the anodic dissolution of iron (**Equation 11**), a high charge transfer resistance (R_{Ct}) indicates a high level of cathodic protection, effectively suppressing the reaction. As R_{ct} decreased, the anodic reaction accelerated, reflecting reduced protection and increased surface

activity.

The two-tiered modeling testing was performed on the same assumed pipeline system from the previous section, assuming the soil resistivity distribution under the low resistivity season. **Figure 12** shows the baseline potential distribution of the assumed system, with a marking at 50km showing where the assumed defect in the pipelines coating will be present.

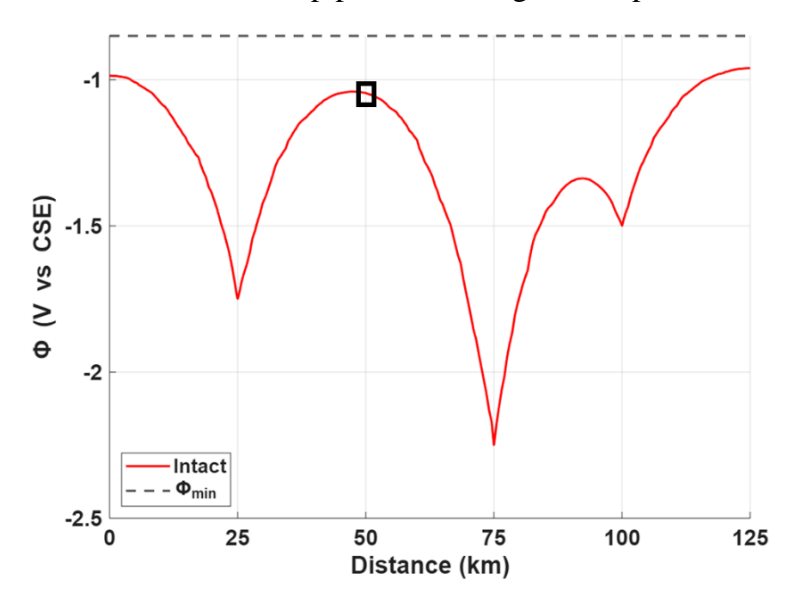


Figure 12: Baseline potential distribution curve used for two-tiered simulation with a defect located at 50km (boxed area)

To investigate the influence of defect size and activity, the local potential profiles are presented in **Figure 13**. **Figure 14** includes the maximum, minimum, and average values of $|Z_T|$ and i_T , providing a quantitative summary of the systems interfacial impedance and transversal current response. The calculated local potential distribution reveals that the detectability of coating holidays depends on both their size and activity level (R_{ct}) . For the 1 cm radius holiday shown in Figure 13a, there was minimal difference in the potential profile between the intact coating and cases where R_{ct} was assumed to be 1e5 or 1e8 Ω cm. A significant deviation in the potential distribution only emerged when the holiday exhibited the highest level of activity. This trend became more pronounced with increasing holiday size, where even moderate activity levels were more likely to influence the system's potential distribution. Suggesting that larger defects would become detectable at lower activity levels, while smaller holidays require higher activity to have the same impact.

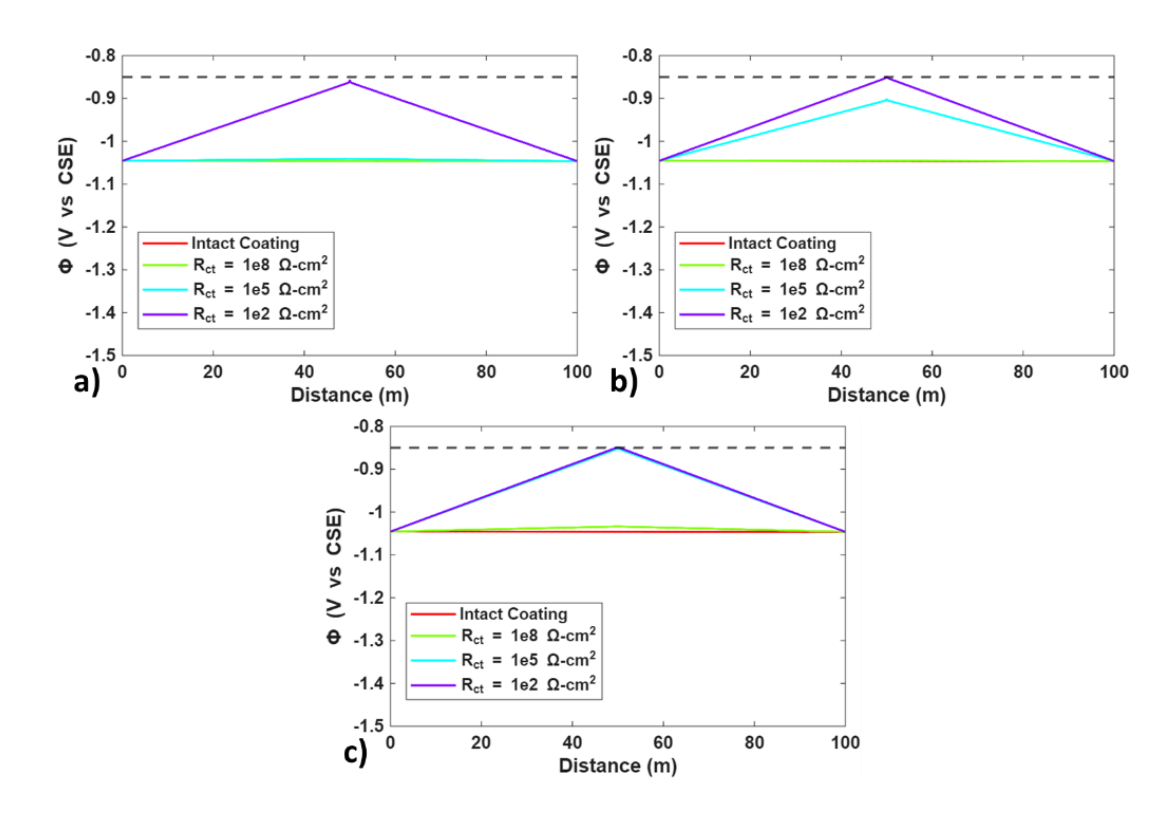


Figure 13: Comparison of the potential distributions for a) defect with 1 cm radius, b) defect with 10 cm radius and b) defect with 50 cm radius at various activity levels

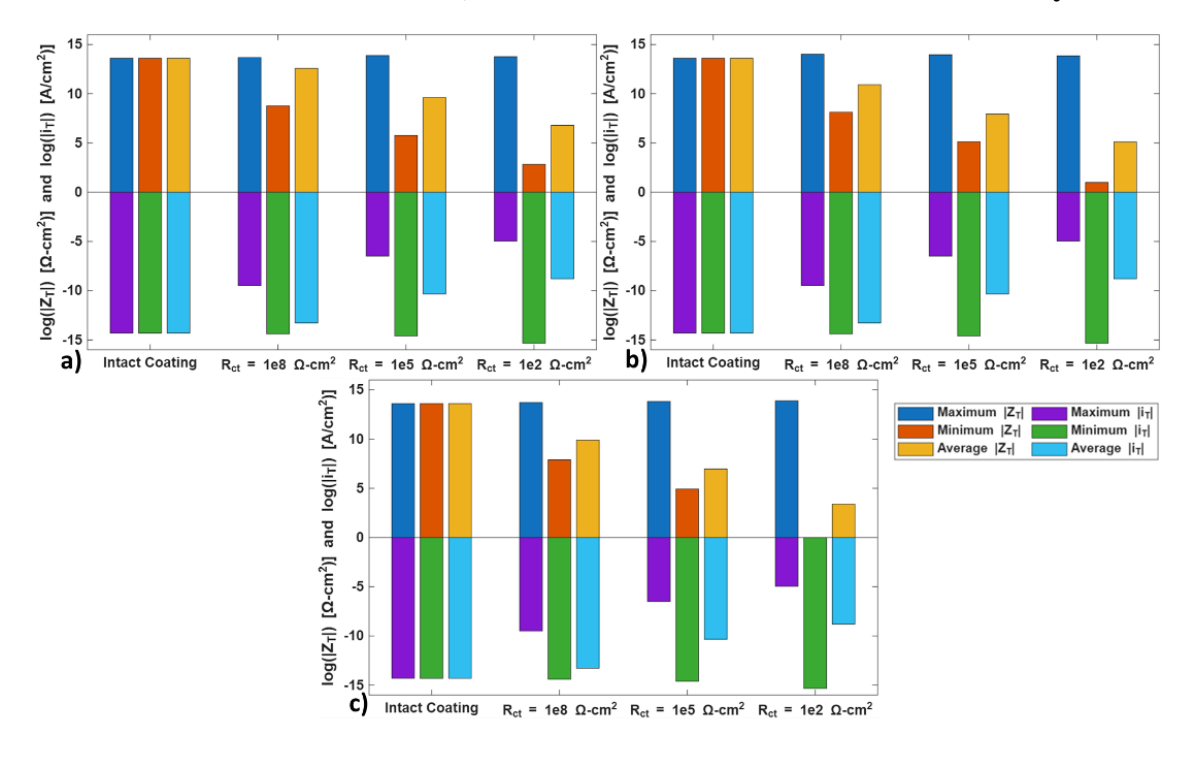


Figure 14: Comparison of the statistical values for $|Z_T|$ and i_T for a) defect with 1 cm radius, b) defect with 10 cm radius and b) defect with 50 cm radius at various activity levels

A comparison of the average $|Z_T|$ values in **Figure 14**, and with the corresponding potential distributions shows that significant changes to the potential profiles occur when the average $|Z_T|$ dropped $10^9 \,\Omega$ cm. Below this threshold, the model predicts a potential distribution that is measurably different from the intact coating scenario. The maximum $|Z_T|$ and minimum i_T are governed by the coating properties. Both parameters exhibit consistent trends: as defect activity increases, the average and minimum $|Z_T|$ decrease proportionally. The i_t displayed an inversely proportional relationship to that of the $|Z_T|$ where the current density would increase in the defective area with increasing activity.

Using the calculated average $|Z_T|$ values for the 100 m region, the potential and interfacial impedance profiles of the system modeled in **Figure 15** were updated accordingly. **Figure 15a** represents the potential profiles incorporating the updated $|Z_T|$ values for the defective region, while **Figure 15b** shows the corresponding interfacial impedance distribution for the system. For the defective region centered around 50 k, the interfacial impedance was assumed to be constant through the region. Four $|Z_T|$ values were chosen two at or above $10^9 \,\Omega$ cm and two values below. This was chosen to see if the trend of the coarser global region had similar behavior to the local simulations.

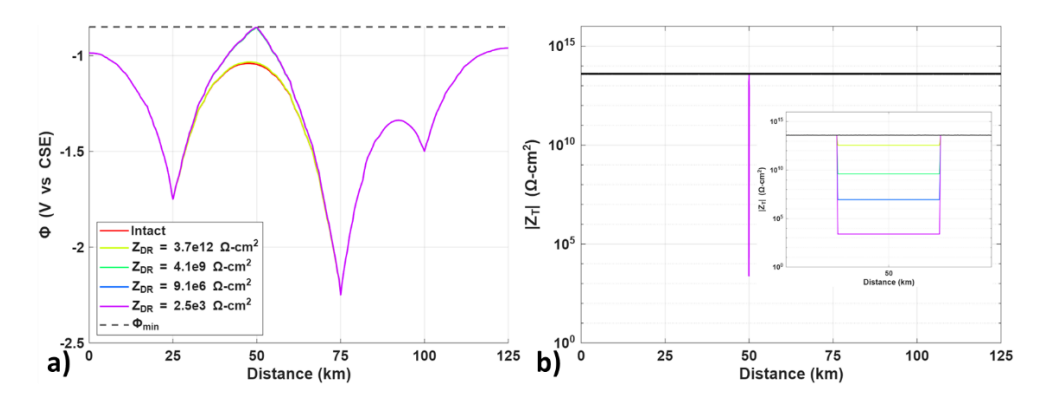


Figure 15: Comparison of the potential distribution for a) various regions with different levels of assumed interfacial impedance distributions using the calculated average $|Z_T|$ values, and b) $|Z_T|$ distribution over the region

Figure 15b reveals a deviation from the trend observed in the local simulations. When $|Z_T|$ was set to 4.1e9 Ω cm, there was a pronounced change in the overall potential profile in the global simulation when contrary to expectations from the local simulations. This discrepancy most likely stems from the assumption that the interfacial impedance region is a single and uniform value over the entire region. By assigning a single $|Z_T|$, the model assumed that each point in that region had an imposed uniform and higher of i_T throughout the region, resulting in an exaggerated shift in the potential profile.

Task 2. Integrating field inspection, theoretical, and experimental data by applying pattern recognition techniques relating the pipeline-coating-soil system with CP

Effective pipeline integrity management requires a holistic understanding of the coupled pipeline coating soil system and its interaction with cathodic protection (CP). Each component contributes unique uncertainties: field inspections (e.g., close interval potential survey, inline inspection)

provide point-wise or distributed evidence of anomalies, whereas theoretical models (e.g., transmission line model) offer mechanistic predictions and experimental data (e.g., soil resistivity tests, coating disbondment) characterize localized behaviors under controlled conditions. Integrating these heterogeneous data sources demands a common framework that can extract patterns across scales and modalities.

As an initial step in this integration, we focused on soil heterogeneity. In earlier work, we conducted a detailed feature analysis to identify independent and informative variables influencing pipeline external corrosion. Building on this foundation, our recent efforts centered on determining the number of underlying soil groups along the pipeline right-of-way (ROW). This was achieved using an in-house developed Bayesian clustering algorithm that accounts for both spatial and statistical behavior of the soil properties. The clustering process begins with identifying the optimal number of clusters for a given soil dataset. Because clustering techniques rely on different data properties, several evaluation measures are used to determine the best fit. For model-based clustering, the Approximate Weight of Evidence Criterion (AWE) is commonly applied. When the Expectation–Maximization (EM) algorithm is employed to estimate the maximum likelihood of a mixture model, an approximation to AWE known as the Bayesian Information Criterion (BIC) becomes particularly useful. The BIC is expressed as

$$BIC = 2loglike(x, \theta) - Mlog(n)$$
 (13)

where, $loglike(x, \theta)$ is the maximized log-likelihood, M is the number of independent parameters to be estimated, and n is the number of data points. A higher BIC value indicates a better model. This is because a well-fitting model yields a higher log-likelihood, while minimizing the number of parameters(M). Using the selected features, the number of clusters was determined by assuming a k-component multivariate Gaussian mixture distribution. **Figure 16** shows the application of this approach to one of the pipeline datasets. The number of clusters (k) was varied from 2 to 20, and the process was iterated 10 times. The knee point of the BIC curve, observed at k = 2, indicates the optimal number of clusters²¹. This result suggests that the soil environment along the studied pipeline segment can be effectively represented by two statistically distinct groups. Such grouping provides a meaningful simplification of the heterogeneous soil system while retaining the dominant features that influence external corrosion risk.

The Bayesian clustering algorithm proceeds by applying the **Expectation–Maximization (EM)** algorithm to extract statistical patterns, such as cluster centers and covariance matrices, from the dataset. This probabilistic framework explicitly accounts for uncertainties in the data, ensuring **robust clustering outcomes**. The results of the clustering analysis are shown in **Figure 17**. **Figure 18a** displays a 2D scatter plot of the first two principal components, with markers representing the cluster centers and contours outlining the Gaussian mixture distributions. The contours visually demonstrate the probabilistic boundaries of each cluster. **Figure 18b** presents a 3D scatter plot of the first three principal components, providing a more comprehensive visualization of the clusters. This plot highlights the separation between cluster groups more distinctly, confirming the effectiveness of the clustering algorithm in capturing the underlying structure of the data.

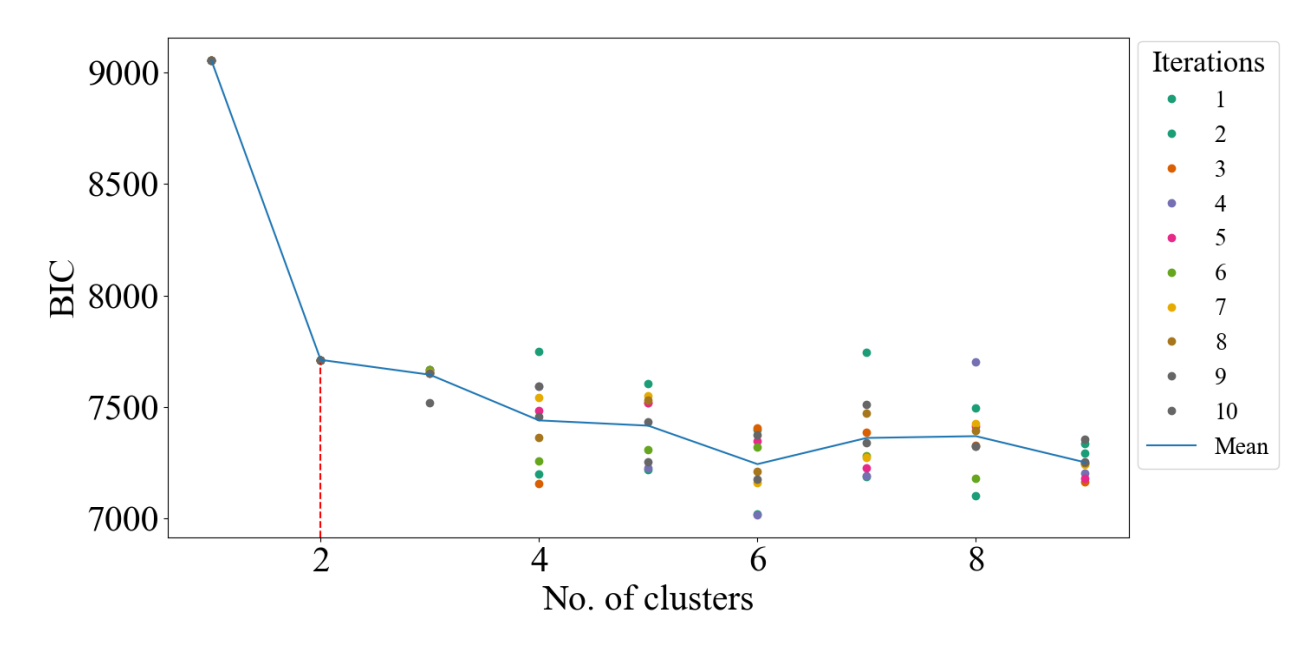


Figure 16: The number of components vs. BIC for full covariance structure, the vertical line indicates the possible optimal number of clusters.

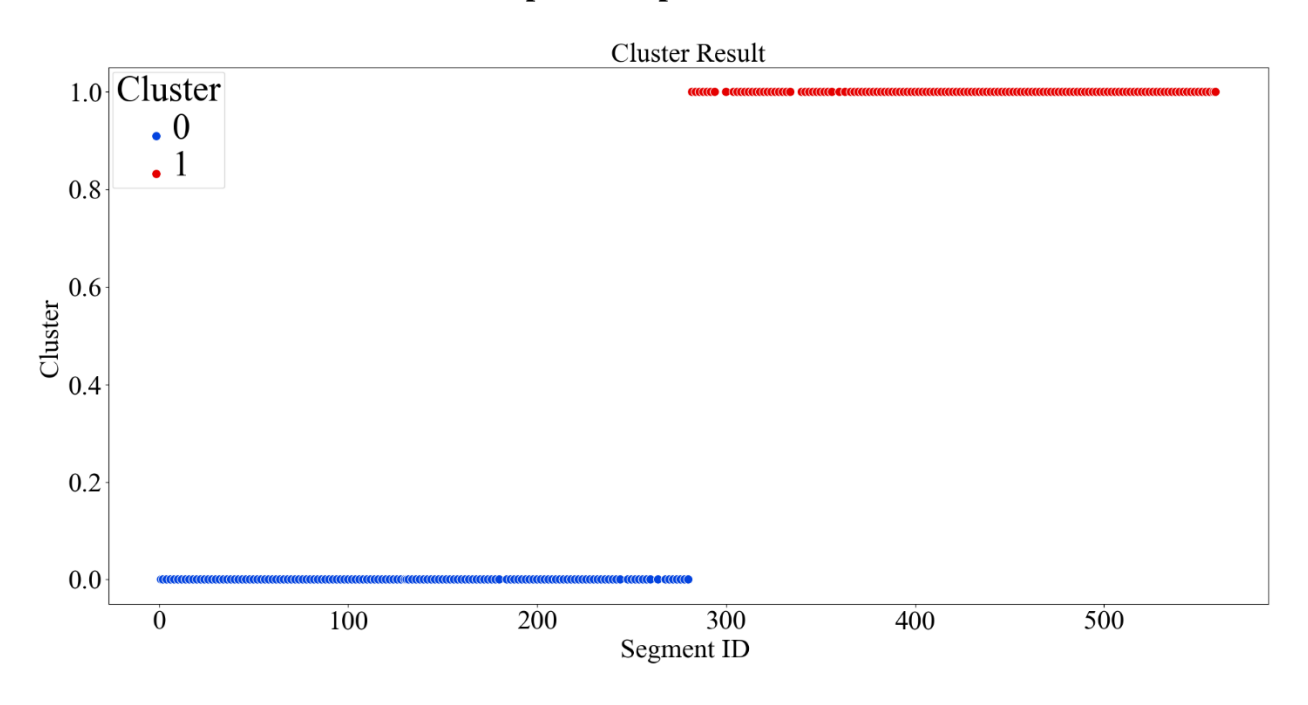


Figure 17: Clustering Results corresponding to k = 2

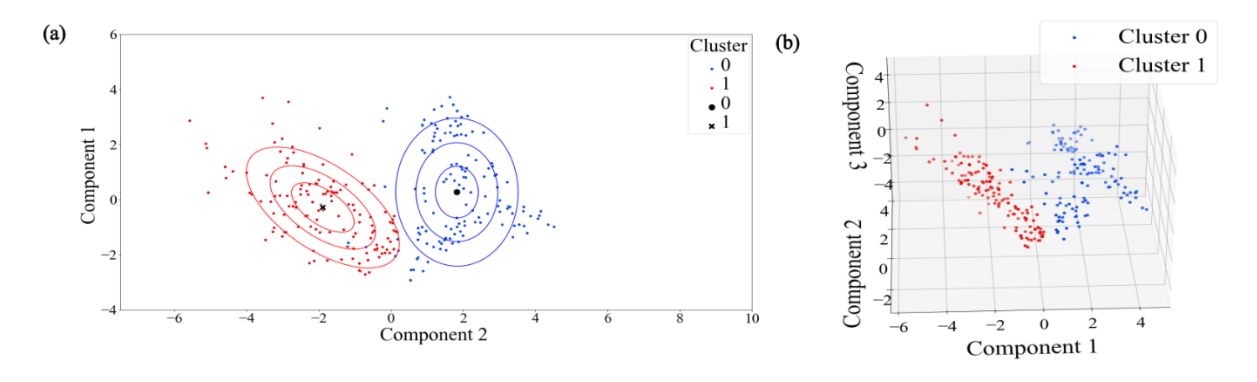


Figure 18: (a) Scatter plots of two principal components with centroid and contour for 2 clusters. (b) 3D scatter plots of three principal components.

Next, we examined the **field inspection data**. The CP potential measurements obtained from a **close interval survey (CIS)** for the study region are visualized in **Figure 19**. Additionally, the **metal loss depth**, as estimated from an inline inspection (ILI) survey, was spatially aligned with the CIS data and overlaid for comparison. The analysis reveals a potential correlation between **soil heterogeneity** and regions of significant metal loss, underscoring the importance of understanding the coupled relationship between **soil properties, CP response, and pipeline integrity**.

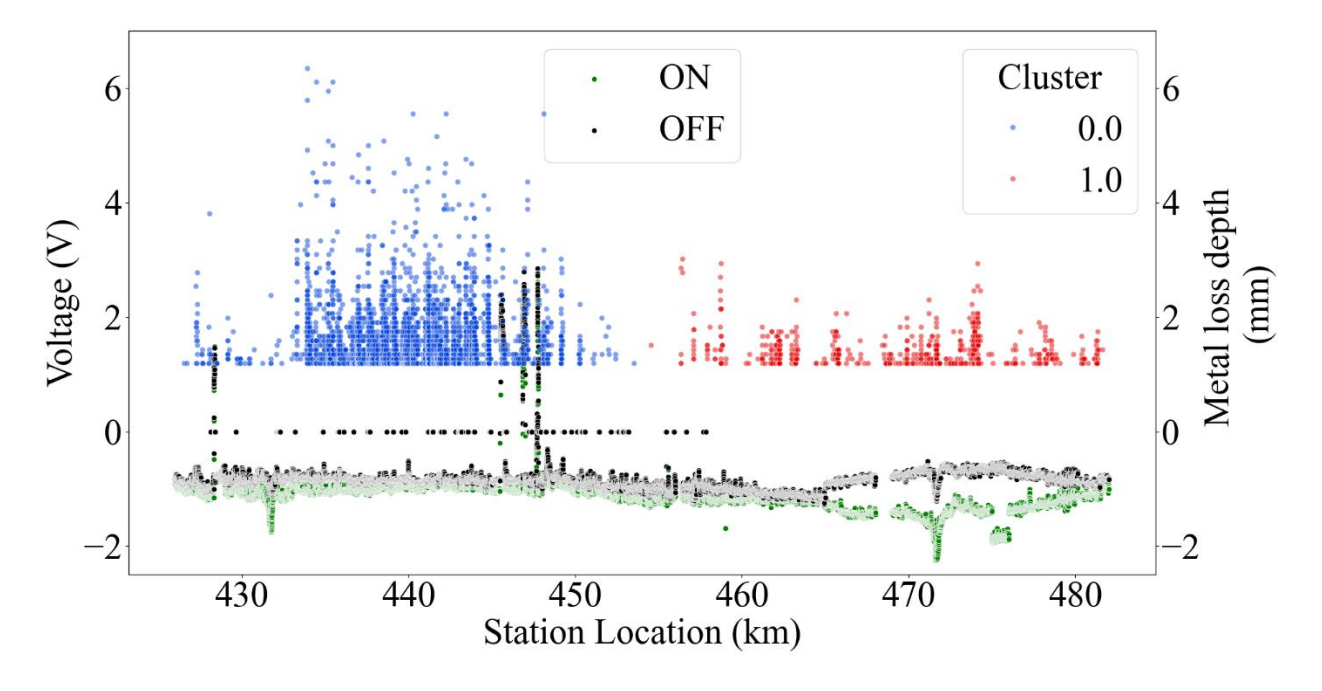


Figure 19: CP potential measured along the pipeline right of way aligned with ILI measured metal loss depth.

Building upon the initial **theoretical framework** developed by the Texas A&M team based on laboratory experiments, we began our analysis of the CIS data by addressing the **global trend** induced by the influence of rectifiers and anodes. The CP potentials originating from rectifiers typically exhibit an **exponential decay** with increasing distance from the source. Based on the dataset, the locations of rectifiers were identified at **431.6467 km** and **471.612 km**, as highlighted

in **Figure 20a**. To prepare the CIS data for detailed analysis anomalous CIS measurements inconsistent with surrounding trends were identified and filtered. Then an exponential decay function was fitted to the potential profiles around the rectifier locations, modeling the **underlying global trend** attributable to current discharge from rectifiers and anodes. The fitted curve, shown in **Figure 20b**, captures the baseline exponential attenuation of CP potentials with distance. This initial verification represents the **first explicit link between theoretical predictions and observed field data**, thereby bridging laboratory models with in-field measurements. Building on this foundation, we developed a **Bayesian framework** to systematically connect theory and observations, as described in **Task 3**.

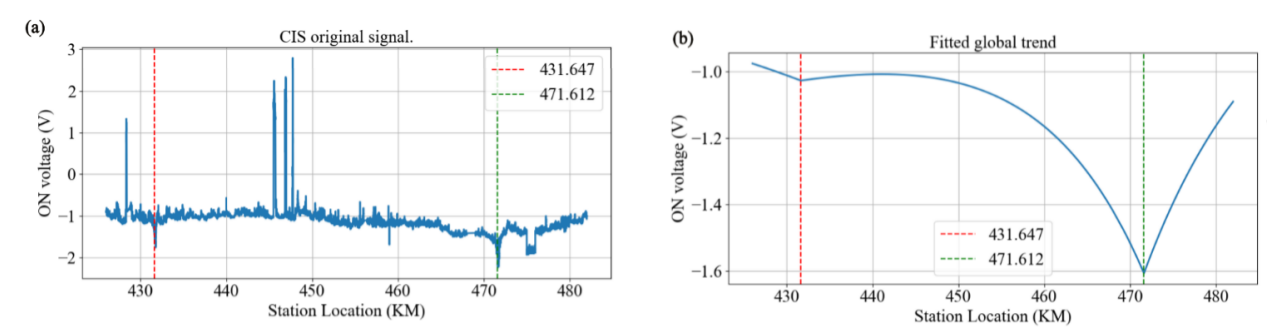


Figure 20 (a): CIS on potential with location of rectifiers influencing the data. (b) Fitted global trend representing potential decay.

Field data validation

To demonstrate feasibility, we first applied our framework to a 56 km pipeline by coupling a forward Transmission Line Model (TLM) with field-measured soil resistivity profiles and using Close Interval Potential Survey (CIPS) voltages as the observed data. The pipeline was discretized into ~28 segments (2 km each), with each segment's coating resistance treated as an unknown inference parameter. We performed Bayesian inversion using the No-U-Turn Sampler (NUTS) in PyMC, yielding posterior distributions and 95 % credible intervals for each segment's impedance as shown in **Figure 21**. As seen in Figure 4(a), the posterior predictive mean potentials (solid line) closely track the observed CIPS voltages, capturing both the overall trend and local fluctuations. **Figure 21b** plots the segment-wise posterior mean coating impedance (solid curve) together with 95 % credible intervals (shaded). Variability in impedance is notably low at the anode locations where concentrated CP current drives the posterior to tighten, while mid-span segments between rectifiers exhibit both lower mean impedances and wider credible intervals, flagging these zones as potential coating degradation hotspots.

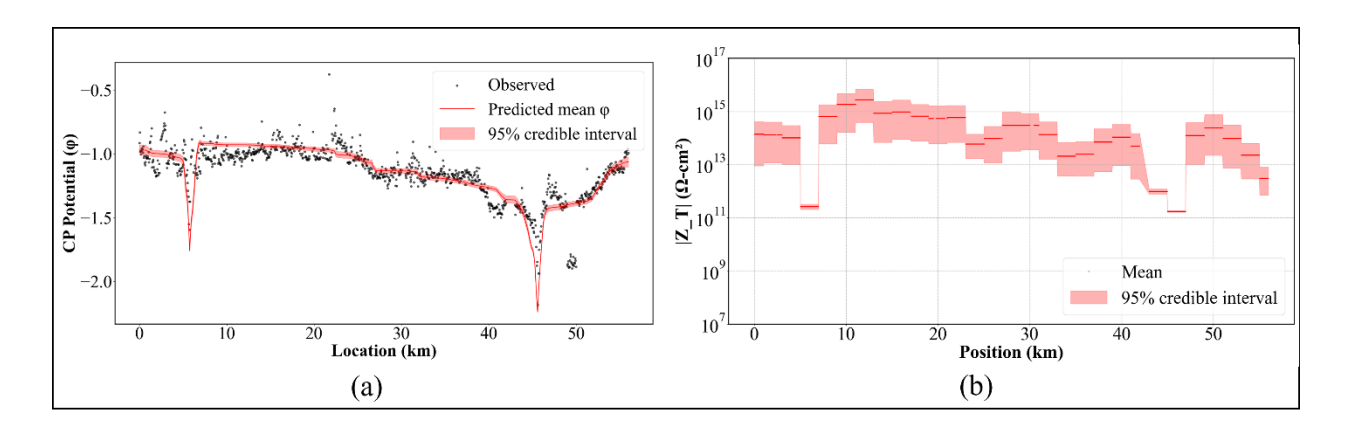


Figure 21: (a) Observed vs Predicted potential (b) Coating Impedance along pipeline right of way

Further validation was done by applying the model to a 110km pipeline as shown in **Figure 22**. The pipe was discretized into 2km segments again resulting in approximately double inference parameters. A major challenge in the Bayesian TLM implementation is the computational time required to sample from a high-dimensional posterior. With ~55 coating-resistance parameters, each NUTS iteration requires solving the TLM forward model (a sparse linear system) 55 times per leapfrog step to evaluate gradients, dramatically increasing per-sample cost. Achieving adequate effective sample sizes typically demands tens of thousands of iterations, further compounding runtime.

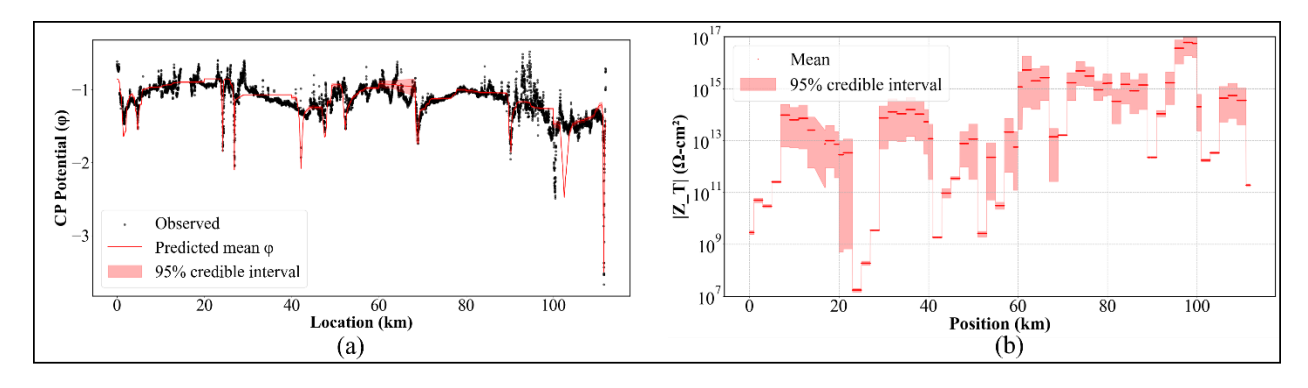


Figure 22: (a) Observed vs Predicted potential, (b) Coating Impedance along pipeline right of way

Future work will focus on replacing the current fixed 2 km segmentation with an adaptive discretization scheme that dynamically refines the mesh where it matters most. In practice, this means allowing users or an uncertainty-driven algorithm to specify regions of interest (e.g., zones with wide posterior credible intervals or suspected coating defects) and automatically subdivide those areas into shorter segments (e.g., 500 m or finer). Coarser segmentation would be retained in regions of low uncertainty to preserve computational efficiency. By coupling this adaptive mesh refinement to the Bayesian updating loop, segment granularity evolves as new CIPS data arrive, the digital twin will deliver higher-resolution impedance estimates exactly where they're needed, guide targeted inspections, and reduce unnecessary computation in benign sections of the pipeline.

Task 3. Development and validation of the Bayesian machine learning framework with experimental and field conditions

The goal of **Task 3** is to establish a Bayesian machine learning framework that integrates theoretical predictions, experimental findings, and field inspection data to quantify the interactions within the pipeline–coating–soil–CP system. The framework was built on the foundation established in earlier tasks:(i) the theoretical models developed by the Texas A&M team that capture current and potential distributions along the pipeline. (ii) experimental datasets characterizing coating degradation, soil resistivity, and electrochemical impedance, and (iii) field inspection data from CIS and ILI surveys.

The proposed framework has three main components 1) the prior distributions 2) the physics engine and 3) the evidence which together yield the posterior distributions of the parameters as shown in **Figure 23**. Our aim is to infer the spatially varying coating impedance from CIPS within a Bayesian framework. Hence the primary latent variable is the per unit coating impedance. To encode the spatial heterogeneity of soil we incorporate the measured soil resistivity as the informative prior, i.e., using it as a mean function for the soil resistivity field.

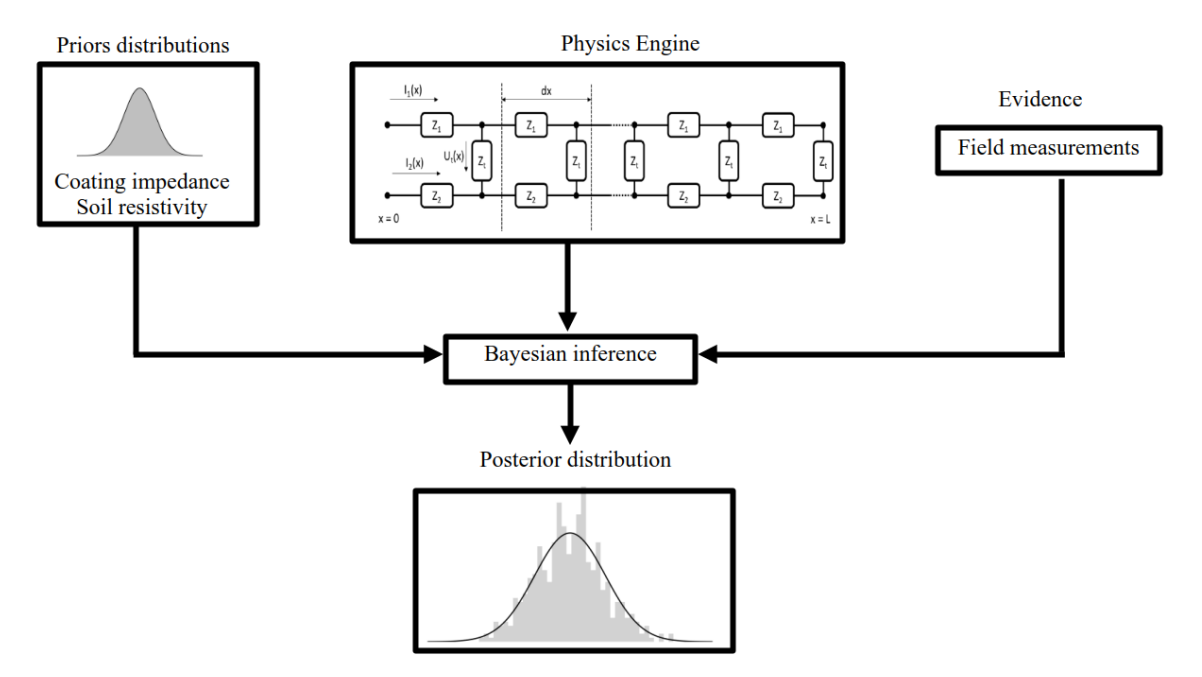


Figure 23: Bayesian Transmission Line Model framework

The TLM forward model produces potential profiles given priors on interface and soil properties, but these are only predictions under assumptions. Incorporating evidence, the measured CIPS potentials, via a realistic likelihood is what turns the model into an inference engine by Bayes' rule,

$$p(\theta|V) = \frac{p(V|\theta)p(\theta)}{p(V)} \tag{14}$$

where θ is the set of all parameters that includes the interface impedance Z_T and soil resistance R_s , and V is the measured CIPS potentials (evidence). Hence the data reweight the prior to yield a posterior over spatial interface impedance and associated predictive intervals. In short, aligning TLM outputs with evidence from the field measurements via a probabilistic framework is the mechanism that moves us from belief to actionable, uncertainty-quantified decisions.

Rather than producing a single deterministic profile of interface impedance, the posterior yields probabilistic spatial maps that capture both the most likely values and the uncertainty associated with them. This is critical in practice: a high posterior probability of low impedance at a given station suggests a degraded interface, while wide credible intervals highlight areas where the evidence is weak or ambiguous. From the posterior we can derive uncertainty bands on interface impedance, compute the probability of degradation at each meter, and generate posterior predictive traces of potential that can be directly compared to observed CIPS data. These outputs enable engineers to move beyond threshold-based interpretations, providing a defensible basis for risk-informed decisions such as excavation prioritization, scheduling follow-up surveys, and refining integrity management strategies. In this way, the posterior is the core outcome of the Bayesian TLM framework it turns physics-based modeling and noisy survey data into actionable, uncertainty-aware guidance for pipeline integrity.

To demonstrate feasibility, we applied our framework to a 50 km pipeline by coupling a forward TLM model with field-measured soil resistivity profiles and using CIPS voltages as the observed data. The pipeline was discretized into segments of approximately 1 km each, with each segment's interface impedance treated as an unknown inference parameter. There are two CP anodes present at locations of 5.76 km and 45.61 km along the right of way (ROW). The posterior distributions and 95 % credible intervals for each segment's impedance as shown in Figure 24. The Bayesian TLM framework reveals spatial variability in coating condition. In several sections, the posterior mean impedance drops by multiple orders of magnitude, indicating zones where the coating is likely degraded. As expected, impedance is lowest at the anode locations, where current enters the system and the credible interval the thinnest. Narrow credible intervals in some stretches suggest high confidence in the inferred impedance, while wider intervals reflect areas where the evidence is weaker, the data noisier, or soil resistivity less constrained. To validate these findings, we overlaid the inline inspection data on metal loss along the ROW as seen in Figure 2 right y axis. Importantly, the low-impedance regions of the lower-bound align with clusters of ILI metal loss supporting the interpretation that where the coating is inferred to be weak, corrosion activity has progressed to measurable wall loss. Conversely, regions of consistently high impedance with tight uncertainty bounds show fewer ILI anomalies, consistent with effective cathodic protection and intact coating.

Further, the posterior distribution of predicted potential with credible intervals (CI) gives a direct check of how well the model captures the observed evidence, as shown in **Figure 25.** The predicted potentials are generated by propagating posterior samples of coating impedance and soil resistivity through the transmission-line model, yielding a full distribution of possible potential traces along the right-of-way. The posterior mean closely follows the measured instant-OFF CIPS voltages, while the shaded 95% credible intervals quantify the range of predictions consistent with both the priors and the observed data. Together, **Figure 24 and 25** confirm that the framework provides

both cause (coating condition via impedance inference) and effect (voltage response via posterior potentials), with uncertainty quantified at each step.

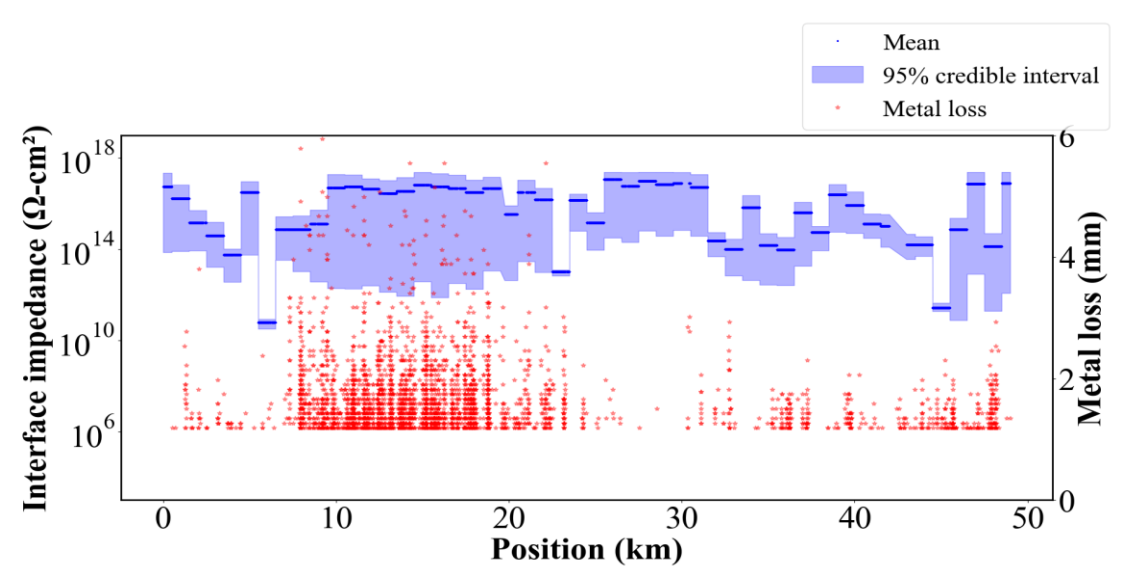


Figure 24: Posterior distribution of interface impedance with 95% credible interval along the 50km pipeline right of way (left-axis) overlaid with inline inspection metal loss (right

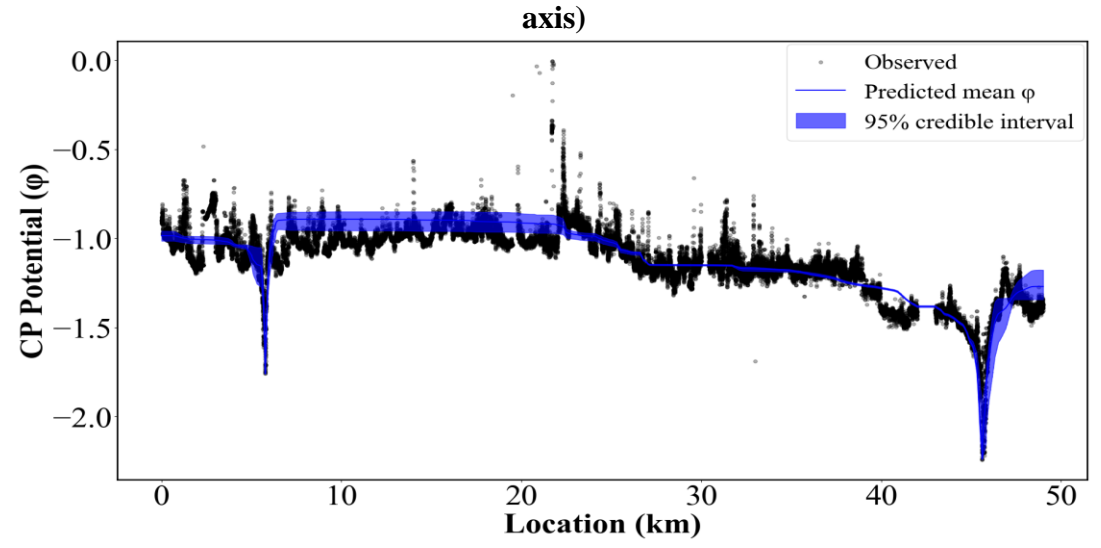


Figure 25: Posterior distribution of predicted potential with 95 % credible interval along the 50km pipeline ROW

Further testing was carried out on a second, longer pipeline of approximately 110 km. This asset was again discretized into ~1 km segments, with each segment's interface impedance treated as an unknown parameter within the Bayesian TLM framework. This system has a greater number of anodes present at locations [1.63, 4.74, 24.25, 26.92, 42.11, 47.57, 52.39, 68.97, 90.19, 100.40, 111.58]. The posterior impedance distributions (**Figure 26**) reveal clear spatial variability. As expected, interface impedance values are lowest near the anode locations, reflecting the strong current injection points and higher protective current density. Between anodes, impedance increases gradually, with localized drops where the framework infers degraded coating. The

posterior predictive distribution of CP potentials (**Figure 27**) also demonstrates strong agreement with measured CIPS voltages. The predictive mean closely follows the observed OFF potentials across the full 110 km, while the 95% predictive bands expand in sections with higher noise or soil variability.

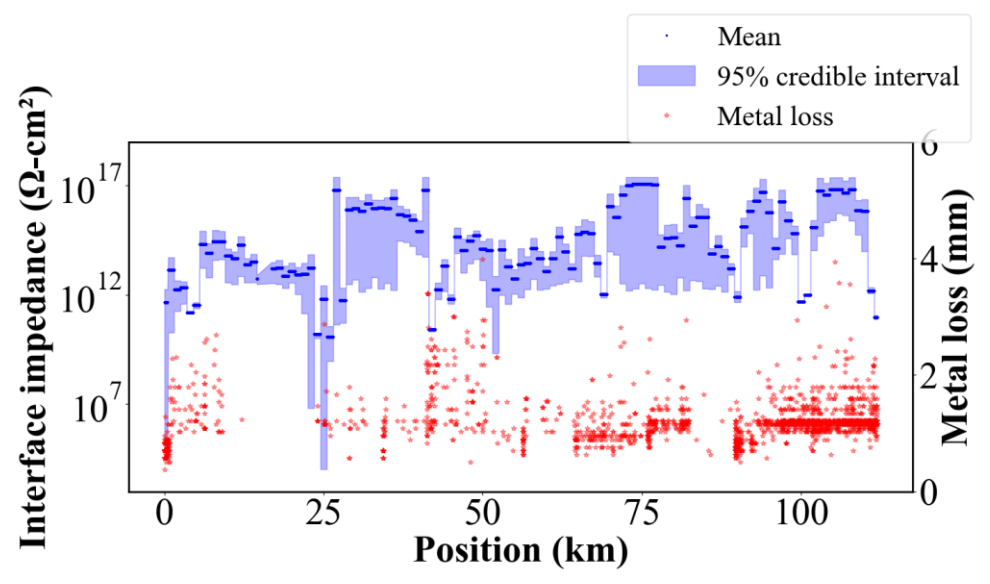


Figure 26: Posterior distribution of interface impedance with 95% credible interval along the 110km pipeline right of way (left-axis) overlaid with inline inspection metal loss (right axis)

While the Bayesian TLM framework provides a rigorous and uncertainty-aware approach for interpreting CIPS data, there are certain limitations. First, the framework is highly dependent on the quality and density of input data. Noisy or poorly synchronized CIPS records can widen posterior uncertainty and reduce effective resolution. Here, resolution refers to the smallest segment length over which the interfacial impedance can be meaningfully inferred; in the present study this was 1 km. The minimum achievable resolution is ultimately constrained by the density of CIPS measurements, since the evidence defines the likelihood. Where data are sparse, the posterior is driven primarily by the prior, and results may simply reflect smoothness assumptions rather than true field variability.

Second, posterior sampling for long pipelines is computationally intensive. With hundreds of inference parameters, Hamiltonian Monte Carlo (HMC) or related sampling methods can become slow, making real-time or near-real-time deployment impractical without algorithmic improvements, surrogate models, or dimensionality reduction strategies. In practice, it is often more efficient to analyze pipelines in smaller sections, where computational demands remain tractable and uncertainty estimates are better constrained.

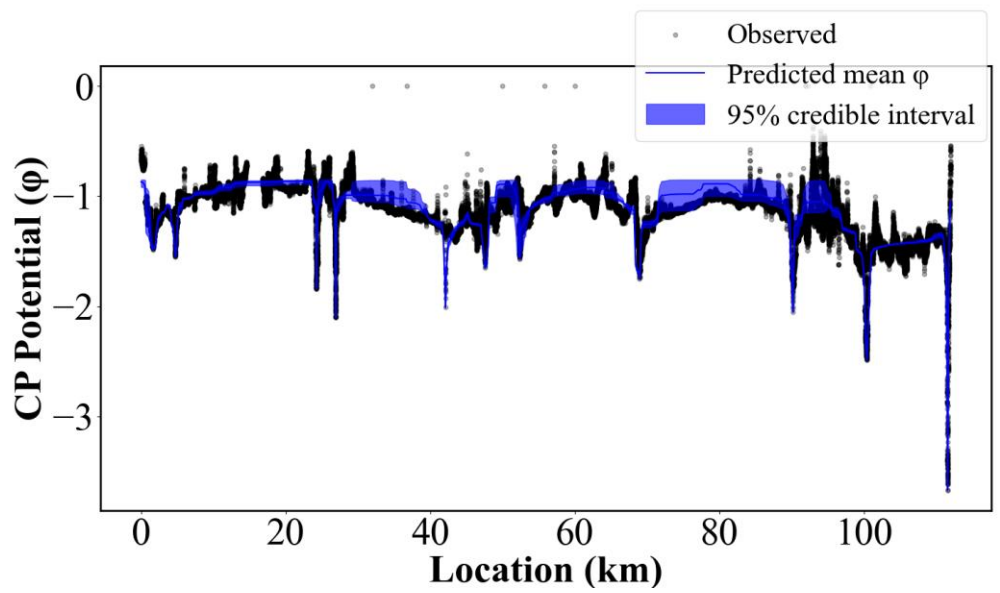


Figure 27: Posterior distribution of predicted potential with 95 % credible interval along the 110km pipeline ROW

Application to two case studies demonstrated the feasibility, scalability, and robustness of the approach. In both cases, the framework captured spatial variability in coating condition, correctly reflecting low impedance at CP anode locations and highlighting degraded segments through impedance drops spanning multiple orders of magnitude.

Further validation was conducted using field datasets collected from the same pipeline in 2018 and 2024. Figure 28 shows the posterior distribution of predicted CP potential (ϕ) with 95% credible intervals along the pipeline ROW for both years. The black markers represent observed CIS measurements, while the colored bands depict model predictions and associated uncertainties.

In 2018 (**Figure 28**, top), the framework reproduced the general CIS trends, but wider credible intervals reflect greater uncertainty due to localized variability and limited prior calibration. By 2024 (**Figure 28**, bottom), the model showed significantly improved agreement with observations, capturing sharper potential drops and localized under-protection zones with narrower credible intervals.

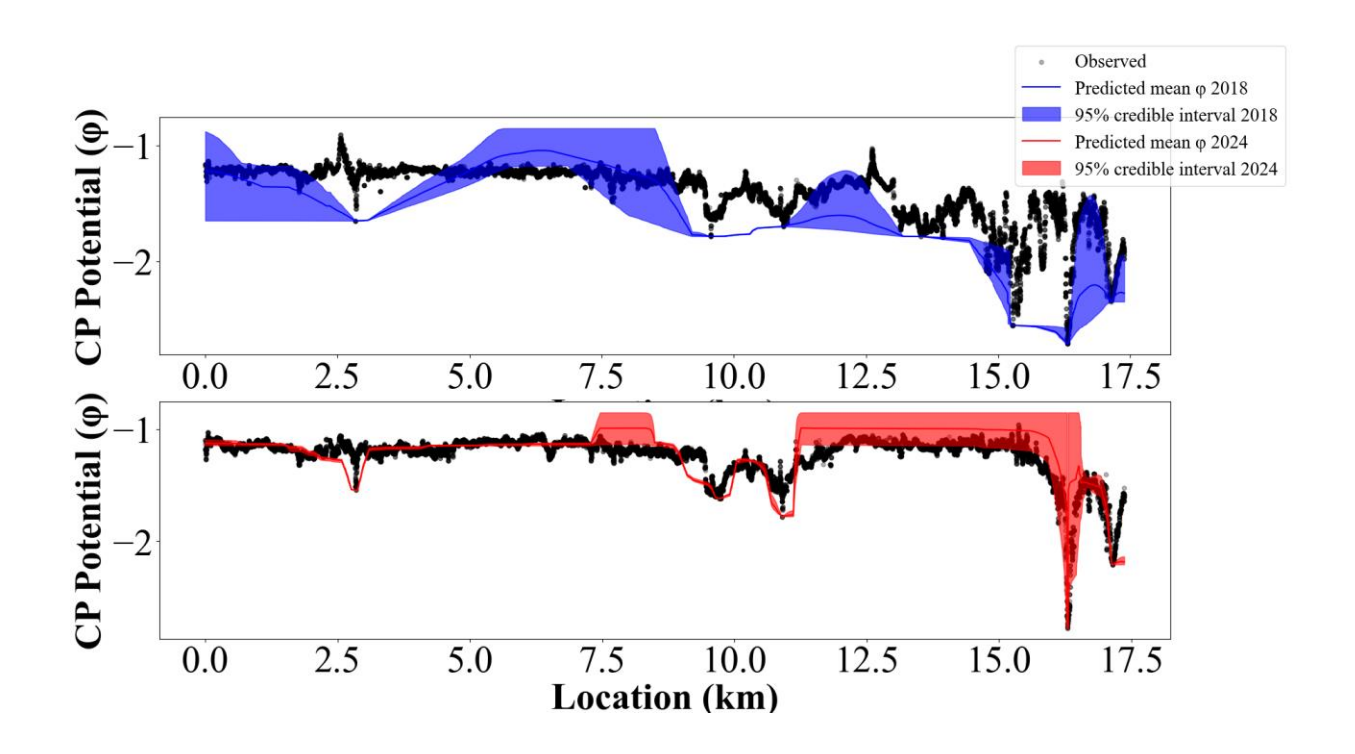


Figure 28: Posterior distribution of predicted CP potential (ϕ) with 95% credible intervals along the same pipeline ROW for 2018 and 2024.

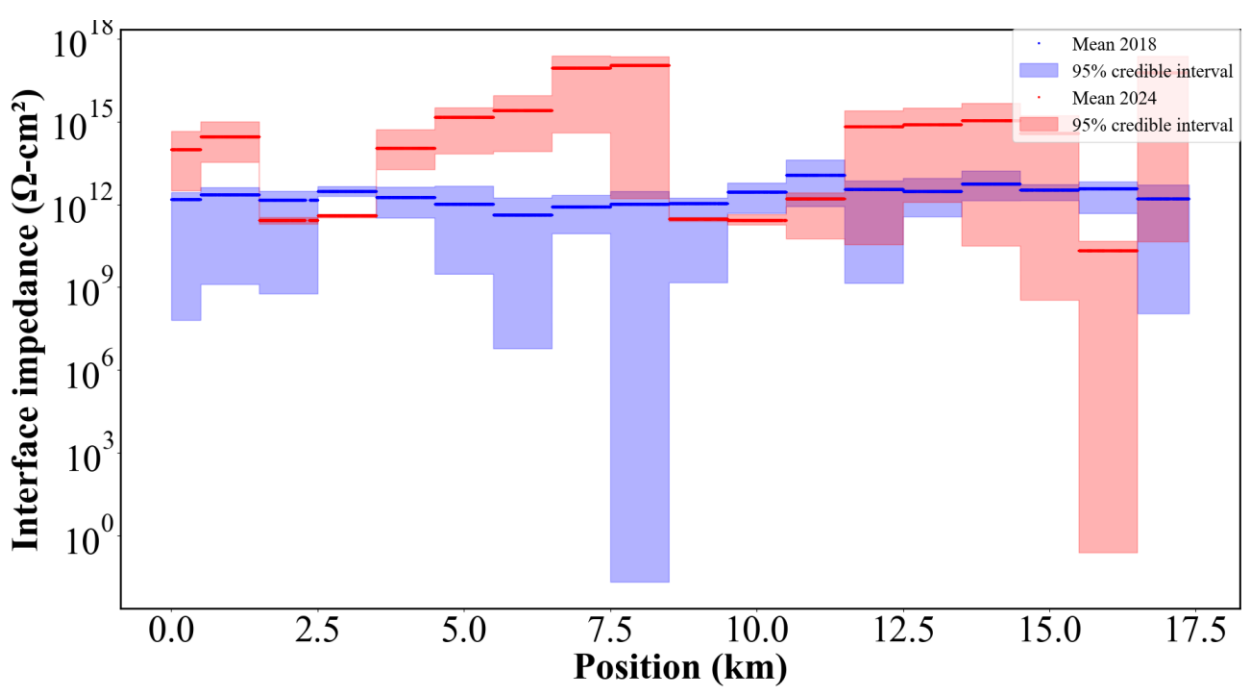


Figure 29: Posterior distribution of interface impedance with 95% credible of the same pipeline for years 2018 and 2024

The **inferred pipeline coating soil interface impedance** was compared across the two survey years. Figure 29 presents the overlay of impedance distributions for 2018 and 2024 along the

pipeline ROW. The results highlight distinct temporal changes in interface behavior. There will be study done in future to better understand the data.

The present study demonstrates the feasibility of the Bayesian TLM framework, and a critical next step is to validate the results through direct field verification of pipeline condition. A test-bed pipeline has already been identified, and planned excavations and inspections are expected to provide the ground-truth data necessary to further validate the methodology.

Task 4 – Development and validation of the methodology for ECDA based on CP levels

Proposal for Non-Destructive Monitoring of Buried Pipeline Health in RELLIS Campus

We will perform a 2 – 3-month monitoring program of non-destructive electrical and electrochemical measurements to assess the integrity of buried pipelines on the RELLIS Campus. We are planning on using established techniques such as: close interval potential survey (CIPS), DC/AC voltage gradient (DCVG/ACVG), and pipeline current mapping (PCM). These techniques will be used to validate a proposed cathodic protection (CP) model developed in the National Corrosion and Materials Reliability Center (NCMRC). Importantly the proposed testing will be concluded with zero disruption to pipeline services and minimal environmental disturbance.

Objectives

Site Preparation and Electrical Connection

- 1. Select target pipeline segments based on history and accessibility.
- 2. Determine if existing CP is present:
 - If CP is absent, we will attach a temporary sacrificial anode to apply local CP.
- 3. Excavate a relatively small area for access (roughly 30 × 30 cm) to expose the pipeline for electrical connection.
- 4. Secure all electrical connections using magnetic clamps (no welding required).
- 5. Backfill the pits and mark locations with temporary flags for easy re-exposure and extraction of electrical connections and anodes

Magnetic Clamps with On/Off Switch Magnetic Clamp with On/Off Switch Magnetic Clamp with On/Off Switch Multiple-Angle Magnetic Clamp with On/Off Switch

Magnetic Clamps

Figure 30: Example of Magnetic clamps to be used for electrical connection

Test Methods

Technique	Purpose
CIPS	Measure the pipe-to-soil potentials in short length intervals (~ 1m)
DC/ACVG	Detect voltage gradients in the soil due to coating defects
PCM	Map current distributions in the pipeline from CP system

Test Protocol and Schedule

Activity	Frequency	Description
NDE Measurements	Weekly	Measurements will be performed weekly for 2 – 3 hours per pipeline segment
Soil Sampling	Monthly	Small samples will be taken from the field and analysis will be performed in the corrosion lab
Model Validation Testing	Weekly	The models output based on the some of the field measurements will be compared with the CIPS data for model validation

Environmental and Safety Considerations

- Limit pit footprint to minimize surface disturbance.
- Refill and restore excavations immediately once connections have been made and after connections are removed when testing has ended.
- Adhere to all safety and excavation protocols

4. Future work

- Continue to update the model with various impedance definitions based on mechanistic analysis of processes occurring at the interface
- Adapt the model for comparison with field data
- Continue EIS testing and building a database of impedance responses of various systems.
 - o Instantaneous EIS vs time-based EIS at OCP.
 - o Effect of coating thickness with and without defects
 - CP testing under all coating conditions and coating types
- Create an empirical relationship between the degradation of coating resistivity based on the level of applied polarization for intact coatings exposed to simulated soil environment.
- Continue to characterize the potential decay for the various systems.
- Create testing protocol and testing matrix for characterizing various defect geometries and types with reflectometry
- Perform Field measurements to validate the methodology for assessing CP in buried pipelines.

References

- 1. Warburg, E. Ueber das Verhalten sogenannter unpolarisirbarer Elektroden gegen Wechselstrom. *Ann Phys* **303**, 493–499 (1899).
- 2. Huang, J. Diffusion impedance of electroactive materials, electrolytic solutions and porous electrodes: Warburg impedance and beyond. *Electrochim Acta* **281**, 170–188 (2018).
- 3. Hinderliter, B. R., Croll, S. G., Tallman, D. E., Su, Q. & Bierwagen, G. P. Interpretation of EIS data from accelerated exposure of coated metals based on modeling of coating physical properties. *Electrochim Acta* **51**, 4505–4515 (2006).
- 4. Bouvet, G., Nguyen, D. D., Mallarino, S. & Touzain, S. Analysis of the non-ideal capacitive behaviour for high impedance organic coatings. *Prog Org Coat* **77**, 2045–2053 (2014).
- 5. Young, L. Anodic oxide films. (No Title) (1961).
- 6. Schiller, C. A. & Strunz, W. *The Evaluation of Experimental Dielectric Data of Barrier Coatings by Means of Different Models. Electrochimica Acta* vol. 46 www.elsevier.com/locate/electacta (2001).
- 7. Schiller, C. A. & Strunz, W. *The Evaluation of Experimental Dielectric Data of Barrier Coatings by Means of Different Models. Electrochimica Acta* vol. 46 www.elsevier.com/locate/electacta (2001).
- 8. De Levie, R. Notes on Gouy Diffuse-Layer Theory. J. Electroanal. Chem vol. 278 (1990).
- 9. Baeckmann, W. Von, Schwenk, W. & Prinz, W. Handbook of Cathodic Corrosion Protection Theory and Practice of Electrochemical Protection Processes (3rd Edition). Preprint at https://app.knovel.com/hotlink/toc/id:kpHCCPTPE1/handbook-cathodic-corrosion/handbook-cathodic-corrosion.
- 10. Morgan, J. Cathodic Protection (2nd Edition). in (NACE International).
- 11. Parker, M. & Peattie, E. G. *Pipeline Corrosion and Cathodic Protection: A Practical Manual for Corrosion Engineers, Technicians, and Field Personnel.* (Gulf Professional Publishing, 1988).
- 12. Eltai, E. O., Scantlebury, J. D. & Koroleva, E. V. Protective properties of intact unpigmented epoxy coated mild steel under cathodic protection. *Prog Org Coat* **73**, 8–13 (2012).
- 13. Zhang, L., Lu, X. & Zuo, Y. *The Influence of Cathodic Polarization on Performance of Two Epoxy Coatings on Steel. Int. J. Electrochem. Sci* vol. 9 www.electrochemsci.org (2014).
- 14. Friedman, S. Electrical properties of soils. *Encyclopedia of Agrophysics. Dordrecht: Springer Netherlands* 242–255 (2011).

- 15. Pozdnyakova, L. A. Electrical Properties of Soils. (University of Wyoming, 1999).
- 16. Samouëlian, A. *et al.* Electrical resistivity survey in soil science: a review. Electrical resistivity survey in soil science: a review .. Soil and Electrical resistivity survey in soil science: a review. *Tillage Research* **83**, 173–193 (2005).
- 17. Kižlo, M. & Kanbergs, A. The causes of the parameters changes of soil resistivity. *Electrical, Control and Communication Engineering* **25**, 43–46 (2009).
- 18. Coelho, V. L. *et al.* The influence of seasonal soil moisture on the behavior of soil resistivity and power distribution grounding systems. *Electric power systems research* **118**, 76–82 (2015).
- 19. Unde, M. G. & Kushare, B. E. Impact of seasonal variation of soil resistivity on safety of substation grounding system. in *Fifth International Conference on Advances in Recent Technologies in Communication and Computing (ARTCom 2013)* 173–182 (IET, 2013).
- 20. Xu, L. Y. & Cheng, Y. F. Experimental and numerical studies of the effectiveness of cathodic protection at corrosion defects on pipelines. *Corros Sci* **78**, 162–171 (2014).
- 21. Q. Zhao, V. Hautamaki and P. Fränt, "20 Q. Zhao, V. Hautamaki and P. Fränti, "Knee Point Detection in BIC for Detecting the Number of Clusters", ACIVS, 2008," in *International conference on advanced concepts for intelligent vision systems*, Berlin, 2008.